

# Electromagnetic Currents and Magnetic Moments in $\chi$ EFT

S. Pastore<sup>a</sup>, L. Girlanda<sup>b,c</sup>, R. Schiavilla<sup>a,d</sup>, M. Viviani<sup>c</sup>, and R.B. Wiringa<sup>e</sup>

<sup>a</sup>*Department of Physics, Old Dominion University, Norfolk, VA 23529, USA*

<sup>b</sup>*Department of Physics, University of Pisa, 56127 Pisa, Italy*

<sup>c</sup>*INFN-Pisa, 56127 Pisa, Italy*

<sup>d</sup>*Jefferson Lab, Newport News, VA 23606*

<sup>e</sup>*Physics Division, Argonne National Laboratory, Argonne, IL 60439*

(Dated: November 1, 2018)

## Abstract

A two-nucleon potential and consistent electromagnetic currents are derived in chiral effective field theory ( $\chi$ EFT) at, respectively,  $Q^2$  (or  $N^2$ LO) and  $eQ$  (or  $N^3$ LO), where  $Q$  generically denotes the low-momentum scale and  $e$  is the electric charge. Dimensional regularization is used to renormalize the pion-loop corrections. A simple expression is derived for the magnetic dipole ( $M1$ ) operator associated with pion loops, consisting of two terms, one of which is determined, uniquely, by the isospin-dependent part of the two-pion-exchange potential. This decomposition is also carried out for the  $M1$  operator arising from contact currents, in which the unique term is determined by the contact potential. Finally, the low-energy constants (LEC's) entering the  $N^2$ LO potential are fixed by fits to the  $np$  S- and P-wave phase shifts up to 100 MeV lab energies.

PACS numbers: 12.39.Fe, 13.40.-f, 21.10.Ky

## I. INTRODUCTION, CONCLUSIONS, AND OUTLOOK

A quantitative understanding of low-energy nuclear physics in terms of *ab initio* calculations in quantum chromodynamics (QCD) is still lacking because of the non-perturbative character of the theory in this regime. However, the chiral symmetry exhibited by QCD severely restricts the form of the interactions of pions among themselves and with other particles [1]. In particular, the pion couples to the baryons, such as nucleons or  $\Delta$ -isobars, by powers of its momentum  $Q$ , and the Lagrangian describing these interactions can be expanded in powers of  $Q/\Lambda_\chi$ , where  $\Lambda_\chi \sim 1$  GeV specifies the chiral-symmetry breaking scale. As a consequence, classes of Lagrangians emerge, each characterized by a given power of  $Q/\Lambda_\chi$  and each involving a certain number of unknown coefficients, so called low-energy constants (LEC's), which are then determined by fits to experimental data (see, for example, the review papers [2] and [3], and references therein).

This approach, known as chiral effective field theory ( $\chi$ EFT), has been used to study two- and many-nucleon interactions [3] and the interaction of electroweak probes with nuclei [4, 5]. Its validity, though, is restricted to processes occurring at low energies. In this sense, it has a more limited range of applicability than meson-exchange or more phenomenological models of these interactions, which in fact quantitatively and successfully account for a wide variety of nuclear properties and reactions up to energies, in some cases, well beyond the pion production threshold (for a review, see Ref. [6]). However, it can be justifiably argued that  $\chi$ EFT puts nuclear physics on a more fundamental basis by providing, on the one hand, a direct connection between QCD and its symmetries, in particular chiral symmetry, and the strong and electroweak interactions in nuclei, and, on the other hand, a practical calculational scheme susceptible, in principle, of systematic improvement.

Recently we derived the nuclear electromagnetic current in a  $\chi$ EFT with explicit pion, nucleon, and  $\Delta$ -isobar degrees of freedom [7]. Formal expressions up to one loop— $N^3$ LO or  $eQ$  in the power counting scheme,  $Q$  generically indicating the low momentum scale, and  $e$  being the electric charge—were obtained in time ordered perturbation theory (TOPT) by employing non-relativistic Hamiltonians implied by the chiral Lagrangian formulation of Refs. [8, 9, 10]. An important aspect of the derivations in Ref. [7] is in the treatment of the reducible diagrams: recoil corrections, which arise from expanding the nucleon energy denominators in these diagrams, were found to partially cancel out the contributions from the irreducible diagrams. When applied to the nucleon-nucleon ( $NN$ ) case, this approach removes explicit energy dependencies, and in fact leads, at least up to one loop ( $N^2$ LO or  $Q^2$ ), to the same potential constructed by Epelbaum *et al.* by the method of the unitary transformation [10]. It also generates  $N^3$ LO currents, which satisfy current conservation with this potential.

One-loop  $\chi$ EFT currents have also been derived, with nucleons and pions only, within the heavy-baryon (HB) formalism by Park *et al.* in Ref. [5], and have been used in calculations of the  $n$ - $p$  [5, 11] and  $n$ - $d$  [12] capture cross sections, spin observables in  $\vec{n}$ - $\vec{p}$  capture [13], and magnetic moments of the deuteron and trinucleons [11], by evaluating the relevant transition matrix elements between wave functions obtained from realistic potentials, *i.e.* in the hybrid approach. Later in the present work we shall show that there are differences between the currents obtained in the HB and TOPT formalisms, some of which have to do with the treatment of reducible diagrams mentioned above (see Sec. IV). We should note that electromagnetic currents in the isoscalar sector were also discussed in Refs. [14, 15], and used in calculations of the deuteron static properties and elastic form factors.

The N<sup>2</sup>LO ( $eQ^0$ ) currents, namely without loop corrections, were used in Ref. [7] to carry out hybrid calculations of the magnetic moments of  $A=2$  and 3 nuclei, and thermal neutron radiative captures on protons and deuterons. To have an estimate of the model dependence due to short-range phenomena, the variation of the predictions was studied as a function of the cutoff parameter  $\Lambda$ , needed to regularize the two-body operators entering the matrix elements, as well as a function of the input potentials. These N<sup>2</sup>LO calculations did not provide a satisfactory description of the experimental data, particularly for the suppressed process  ${}^2\text{H}(n, \gamma){}^3\text{H}$ , which exhibited a pronounced sensitivity to variations in  $\Lambda$ . This clearly pointed to the need of including loop corrections.

This work represents the next stage in the program initiated in Ref. [7]. It constructs, consistently within the  $\chi$ EFT framework, a  $NN$  potential and one- and two-body currents up to N<sup>3</sup>LO, with the ultimate aim of studying electromagnetic properties and radiative captures in few-nucleon systems at this order. More specifically, it fulfills two objectives. The first is the construction, in dimensional regularization, of a  $NN$  potential at one loop (Sec. II). The nine LEC's— $C_S$  and  $C_T$  at  $Q^0$ , and  $C_1, \dots, C_7$  at  $Q^2$  in the notation of Ref. [10]—which enter the potential at this order are determined by fitting the  $np$  S- and P-wave phase shifts up to 100 MeV lab energies, obtained in the recent partial-wave analysis of Gross and Stadler [16] (Sec. V). Differences between the present version of the potential and that obtained by Epelbaum and collaborators [17] are not substantive, since they relate to the use of a different form for the regulator in the solution of the Lippmann-Schwinger equation and the adoption, in their case, of the older Nijmegen phase-shift analysis [18] for the determination of the LEC's.

The second objective is to carry out the renormalization (in dimensional regularization) of the tree-level and one-loop two-body currents, and to derive the complete set of contact currents at N<sup>3</sup>LO (Sec. III). Those implied by minimal substitution in the contact interaction Hamiltonians with two gradients of the nucleon fields were in fact obtained in Ref. [7]. However, in that work non-minimal couplings were not considered: we remedy that omission here. Lastly, in the present study we also derive (renormalized) expressions for the magnetic dipole ( $M1$ ) operator at N<sup>3</sup>LO (Secs. IV and VI). We find it convenient to separate, in the contributions from loop corrections, a term dependent on the center-of-mass position of the two nucleons [19, 20], which is uniquely determined via current conservation by the isospin-dependent part of the two-pion-exchange chiral potential, and a translationally-invariant term. The latter has a different isospin structure than that of Ref. [5] for the reason mentioned earlier.

This decomposition is carried out also for the  $M1$  operator generated by the N<sup>3</sup>LO contact currents. The center-of-mass dependent term is related to the contact potential, specifically the part of it which is momentum-dependent and therefore does not commute with the charge operator. However, the translationally invariant contact  $M1$  operator depends on two LEC's. There are also N<sup>3</sup>LO (translationally invariant)  $M1$  corrections at tree level, involving one-pion exchange, which depend on three additional LEC's. These five LEC's could be fixed either by reproducing a combination of nucleon and nuclear data—for example, pion-photoproduction data on a single nucleon along with the deuteron magnetic moment and cross section for  $np$  radiative capture at thermal energies—or by relying exclusively on nuclear data—by fitting, in addition to the observables mentioned earlier, also the trinucleon magnetic moments and radii. In this respect, we note that there appear to be no three-body currents entering at N<sup>3</sup>LO (namely,  $eQ^{-2}$  in  $A=3$  systems) [21].

The stage is now set for carrying out a consistent  $\chi$ EFT calculation of electromagnetic

properties and reactions in  $A=2-4$  nuclei. The thermal neutron  $n$ - $d$  and  $n$ - $^3\text{He}$  and keV  $p$ - $d$  captures are especially interesting, since the  $M1$  transitions connecting the continuum states to the hydrogen- and helium-isotope bound states are inhibited at the one-body (LO) level. As a result, the cross sections for these processes are significantly enhanced by many-body components in the electromagnetic current operator [22, 23]. Work along these lines is in progress. However, it remains to be seen whether the  $N^3\text{LO}$  operators derived in this study will reduce the sensitivity to short-range physics found in the  $N^2\text{LO}$  hybrid calculations (for the  $n$ - $d$  case) referred to earlier, and bring theory into satisfactory agreement with experiment.

## II. $NN$ POTENTIAL AT $N^2\text{LO}$

This section deals with the construction of the  $NN$  potential in  $\chi\text{EFT}$  up to order  $Q^2$ , or  $N^2\text{LO}$ . It is derived by retaining only pions and nucleons as degrees of freedom—the inclusion of explicit  $\Delta$ -isobar degrees of freedom is deferred to a later work [21]. The formalism as well as the techniques we adopt have already been described in Ref. [7], and we will not reformulate them here.

In Fig. 1 we show the diagrams illustrating the contributions occurring up to  $N^2\text{LO}$ . At LO ( $Q^0$ ) there is a contact interaction, panel a), along with the one-pion-exchange (OPE) contribution, panel b). At  $N^2\text{LO}$  we distinguish among three different categories, which are: i) contact interactions involving two gradients acting on the nucleons' fields, panel c); ii) two-pion-exchange loop contributions, panels d)-f); and iii) loop corrections to the LO contact interaction, panels g) and i), and to the OPE contribution, panel h). Note that in the figure we display only one among the possible time orderings.

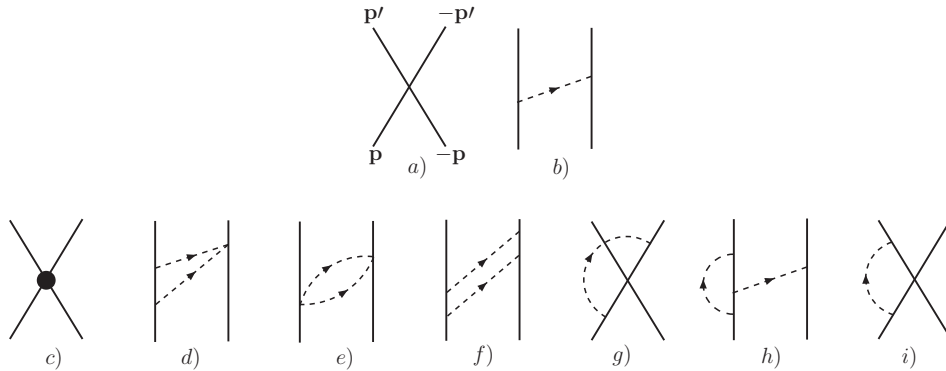


FIG. 1: Diagrams illustrating contributions to the  $NN$  potential entering at LO ( $Q^0$ ), panels a) and b), and  $N^2\text{LO}$  ( $Q^2$ ), panels c)-i). Nucleons and pions are denoted by solid and dashed lines, respectively. The filled circle in panel c) represents the vertex from contact Hamiltonians containing two gradients of the nucleons' fields. Only one among the possible time orderings is shown for each contribution with more than one vertex.

The time ordered diagrams of panels a)-e) are irreducible, while those of panels f)-g) have both reducible and irreducible character. In order to avoid double counting of the reducible contributions due to insertion of the LO potential into the Lippmann-Schwinger equation, the  $NN$  potential is defined as the sum of the irreducible diagrams only.

The evaluation of the  $NN$  potential is carried out in the static limit. Corrections to this approximation arise from kinetic energies of nucleons, and are referred to as recoil corrections. The latter are not accounted for in the Lippmann-Schwinger equation in which only the static potential is iterated. Hence they have been included below along with the irreducible contributions. The resulting potential is in agreement with that obtained by Epelbaum *et al.* in Ref. [10]. Special treatment is reserved for the diagrams of panels h) and i), which are discussed later in this section.

### A. Formal expressions

In what follows we use the notation introduced in Ref. [7]. In particular, the potential is obtained in the center-of-mass frame where the nucleons' initial and final relative momenta are  $\mathbf{p}$  and  $\mathbf{p}'$ , respectively. We also define  $\mathbf{k} = \mathbf{p}' - \mathbf{p}$ ,  $\mathbf{K} = (\mathbf{p}' + \mathbf{p})/2$ ,  $\omega_k = \sqrt{k^2 + m_\pi^2}$ , and

$$\int_{\mathbf{p}} \equiv \int \frac{d\mathbf{p}}{(2\pi)^3} . \quad (2.1)$$

In the remainder of this section we will refer to the panels in Fig. 1.

The diagram illustrated by panel a) gives rise to the LO order contact potential  $v^{\text{CT0}}$ , which is expressed in terms of two LEC's  $C_S$  and  $C_T$  as

$$v^{\text{CT0}} = C_S + C_T \boldsymbol{\sigma}_1 \cdot \boldsymbol{\sigma}_2 , \quad (2.2)$$

while that of panel b) leads to the standard OPE potential,

$$v^\pi(\mathbf{k}) = -\frac{g_A^2}{F_\pi^2} \boldsymbol{\tau}_1 \cdot \boldsymbol{\tau}_2 \frac{\boldsymbol{\sigma}_1 \cdot \mathbf{k} \boldsymbol{\sigma}_2 \cdot \mathbf{k}}{\omega_k^2} . \quad (2.3)$$

Next we consider the contributions arising from panel c). There is a number of contact Hamiltonians involving two gradients acting on the nucleons' fields compatible with the required symmetries of the underlying theory. In fact, the list of fourteen given in Ref. [10] and reported in Appendix D of Ref. [7] is redundant, since relations exist among the terms proportional to  $C'_4$ ,  $C'_5$ , and  $C'_6$ , and those proportional to  $C'_7$ ,  $C'_8$ ,  $C'_{10}$ ,  $C'_{11}$  (see Appendix A). We will not enforce these in the following, since, in any case, the contact Hamiltonians (all twelve of them) lead (in the center-of-mass frame) to seven independent operator structures in the potential, each multiplied by a coefficient which is a linear combination of LEC's. Specifically,

$$\begin{aligned} v^{\text{CT2}}(\mathbf{k}, \mathbf{K}) = & C_1 k^2 + C_2 K^2 + (C_3 k^2 + C_4 K^2) \boldsymbol{\sigma}_1 \cdot \boldsymbol{\sigma}_2 + i C_5 \frac{\boldsymbol{\sigma}_1 + \boldsymbol{\sigma}_2}{2} \cdot \mathbf{K} \times \mathbf{k} \\ & + C_6 \boldsymbol{\sigma}_1 \cdot \mathbf{k} \boldsymbol{\sigma}_2 \cdot \mathbf{k} + C_7 \boldsymbol{\sigma}_1 \cdot \mathbf{K} \boldsymbol{\sigma}_2 \cdot \mathbf{K} , \end{aligned} \quad (2.4)$$

where the  $C_i$ 's ( $i = 1, \dots, 7$ ) are linear combinations of the  $C'_i$ 's ( $i = 1, \dots, 14$ ), given by

$$\begin{aligned} C_1 &= C'_1 - C'_3 + C'_2/2 , \\ C_2 &= 4 C'_1 - 4 C'_3 - 2 C'_2 , \\ C_3 &= C'_9 + C'_{12}/2 - C'_{14} , \\ C_4 &= 4 C'_9 - 2 C'_{12} + 4 C'_{14} , \\ C_5 &= 2 C'_5 - 4 C'_4 - 2 C'_6 , \\ C_6 &= C'_7 + C'_8 + C'_{10}/2 + C'_{11}/2 - C'_{13} , \\ C_7 &= 4 C'_7 + 4 C'_8 - 2 C'_{10} - 2 C'_{11} + 4 C'_{13} , \end{aligned} \quad (2.5)$$

and, as per the comment above, one should keep in mind that any single one of the terms proportional to  $C'_4$ ,  $C'_5$ , and  $C'_6$  ( $C'_7$ ,  $C'_8$ ,  $C'_{10}$ , and  $C'_{11}$ ) can be reduced to a combination of the remaining ones by a simple redefinition of the LEC's.

The two-pion-exchange loop diagrams of panels d)-f) generate the following contribution:

$$\begin{aligned} v^{2\pi}(\mathbf{k}) &= v_d(k) + v_e(k) + v_f(\mathbf{k}) \\ &= \frac{g_A^2}{F_\pi^4} \boldsymbol{\tau}_1 \cdot \boldsymbol{\tau}_2 \int_{\mathbf{p}} \frac{p^2 - k^2}{\omega_+ \omega_- (\omega_+ + \omega_-)} - \frac{1}{8 F_\pi^4} \boldsymbol{\tau}_1 \cdot \boldsymbol{\tau}_2 \int_{\mathbf{p}} \frac{(\omega_+ - \omega_-)^2}{\omega_+ \omega_- (\omega_+ + \omega_-)} \\ &\quad - \frac{g_A^4}{2 F_\pi^4} \int_{\mathbf{p}} \frac{\omega_+^2 + \omega_+ \omega_- + \omega_-^2}{\omega_+^3 \omega_-^3 (\omega_+ + \omega_-)} \left[ \boldsymbol{\tau}_1 \cdot \boldsymbol{\tau}_2 (p^2 - k^2)^2 + 6 \boldsymbol{\sigma}_1 \cdot (\mathbf{k} \times \mathbf{p}) \boldsymbol{\sigma}_2 \cdot (\mathbf{k} \times \mathbf{p}) \right], \end{aligned} \quad (2.6)$$

where  $\omega_\pm = \sqrt{(\mathbf{p} \pm \mathbf{k})^2 + 4 m_\pi^2}$ . Note that recoil corrections to the reducible box diagrams have been included in the expressions above (for a detailed discussion of this aspect of the present study, see Section VI of Ref. [7]). These recoil terms need also be accounted for when dealing with loop corrections to the LO contact and OPE interactions. The resulting contributions, panels g) and h), are then found to be

$$v_g = \frac{4 g_A^2}{3 F_\pi^2} C_T \boldsymbol{\tau}_1 \cdot \boldsymbol{\tau}_2 \boldsymbol{\sigma}_1 \cdot \boldsymbol{\sigma}_2 \int_{\mathbf{p}} \frac{p^2}{\omega_p^3}, \quad (2.7)$$

$$v_h(\mathbf{k}) = -\frac{g_A^4}{3 F_\pi^4} \frac{\boldsymbol{\tau}_1 \cdot \boldsymbol{\tau}_2}{\omega_k^2} \boldsymbol{\sigma}_1 \cdot \mathbf{k} \boldsymbol{\sigma}_2 \cdot \mathbf{k} \int_{\mathbf{p}} \frac{p^2}{\omega_p^3}, \quad (2.8)$$

The potential constructed so far is in agreement with that obtained by Epelbaum *et al.* in Ref. [10] by the method of unitary transformations, but for an overall factor of  $+8/3$  rather than  $-1/3$  in Eq. (2.8).

Lastly, we consider the diagram illustrated in panel i), which has both reducible and irreducible parts. The former describe interactions involving “dressed nucleons”. We do not take into account recoil corrections arising from the pion emitted and reabsorbed by the same nucleon. Hence, for diagram i) we retain the irreducible part only, and obtain

$$v_i = \frac{g_A^2}{F_\pi^2} (3 C_S - C_T \boldsymbol{\sigma}_1 \cdot \boldsymbol{\sigma}_2) \int_{\mathbf{p}} \frac{p^2}{\omega_p^3}. \quad (2.9)$$

Again, this approach leads to a result which differs from that reported in Ref. [10] for this diagram, specifically the term proportional to  $C_S$  in Eq. (2.9) is absent, while that proportional to  $C_T$  is multiplied by  $-4 (g_A^2/F_\pi^2)$  rather than  $-(g_A^2/F_\pi^2)$ . However, as it will become clear in the next section, these differences—for diagrams h) and i)—do not affect the definition of the renormalized potential, since they only lead to differences in the renormalization of the LEC's  $C_S$ ,  $C_T$ , and  $g_A$ .

## B. Renormalization

The potential defined in the previous section contains ultraviolet divergencies which need to be removed by a proper renormalization procedure. In order to isolate these divergencies, the kernels of the N<sup>2</sup>LO contributions have been evaluated using dimensional regularization, and the relevant integration formulae are listed in Appendix B. Here we sketch the

regularization procedure of the various contributions, and give the final expression for the renormalized  $NN$  potential.

As an example, we discuss, in some detail, the regularization of the two-pion-exchange contribution of Eq. (2.6). In terms of the kernels  $L(k)$ ,  $I^{(2n)}(k)$  and  $J^{(2n)}(k)$  defined in Appendix B, it reads as

$$v^{2\pi}(\mathbf{k}) = - \frac{1}{8 F_\pi^4} \boldsymbol{\tau}_1 \cdot \boldsymbol{\tau}_2 \left[ L(k) - 8 g_A^2 [I^{(2)}(k) - k^2 I^{(0)}(k)] + 4 g_A^4 [J^{(4)}(k) - 2 k^2 J^{(2)}(k) + k^4 J^{(0)}(k)] \right] - \frac{3 g_A^4}{F_\pi^4} (\boldsymbol{\sigma}_1 \times \mathbf{k})_i (\boldsymbol{\sigma}_2 \times \mathbf{k})_j J_{ij}^{(2)}(k) . \quad (2.10)$$

By inserting the explicit expressions of these kernels in the previous equation, we obtain

$$v^{2\pi}(\mathbf{k}) = \bar{v}^{2\pi}(\mathbf{k}) + \boldsymbol{\tau}_1 \cdot \boldsymbol{\tau}_2 P_2(k) + \left( k^2 \boldsymbol{\sigma}_1 \cdot \boldsymbol{\sigma}_2 - \boldsymbol{\sigma}_1 \cdot \mathbf{k} \boldsymbol{\sigma}_2 \cdot \mathbf{k} \right) P_0 , \quad (2.11)$$

where the renormalized (finite) part of the two-pion-exchange potential, denoted by  $\bar{v}^{2\pi}(\mathbf{k})$ , is given by

$$\bar{v}^{2\pi}(\mathbf{k}) = \frac{1}{48\pi^2 F_\pi^4} \boldsymbol{\tau}_1 \cdot \boldsymbol{\tau}_2 G(k) \left[ 4m_\pi^2(1 + 4g_A^2 - 5g_A^4) + k^2(1 + 10g_A^2 - 23g_A^4) - \frac{48 g_A^4 m_\pi^4}{4 m_\pi^2 + k^2} \right] + \frac{3 g_A^4}{8\pi^2 F_\pi^4} G(k) \left( k^2 \boldsymbol{\sigma}_1 \cdot \boldsymbol{\sigma}_2 - \boldsymbol{\sigma}_1 \cdot \mathbf{k} \boldsymbol{\sigma}_2 \cdot \mathbf{k} \right) , \quad (2.12)$$

with

$$G(k) = \frac{\sqrt{4 m_\pi^2 + k^2}}{k} \ln \frac{\sqrt{4 m_\pi^2 + k^2} + k}{\sqrt{4 m_\pi^2 + k^2} - k} , \quad (2.13)$$

where the loop function  $G(k)$  defined here differs by a factor two from that given in Ref. [10].

The divergencies are lumped into the polynomials  $P_2(k)$  (of order two) and constant  $P_0$ :

$$P_2(k) = - \frac{1}{24\pi^2 F_\pi^4} \left[ m_\pi^2 \left[ 4 + 22g_A^2 - 29g_A^4 - 9g_A^2(2 - 5g_A^2) \left( -\frac{2}{\epsilon} + \gamma - \ln \pi + \ln \frac{m_\pi^2}{\mu^2} \right) \right] + \frac{4}{3} k^2 \left[ 1 + 7g_A^2 - 9g_A^4 - \frac{3}{8} (1 + 10g_A^2 - 23g_A^4) \left( -\frac{2}{\epsilon} + \gamma - \ln \pi + \ln \frac{m_\pi^2}{\mu^2} \right) \right] \right] , \quad (2.14)$$

$$P_0 = \frac{3 g_A^4}{8\pi^2 F_\pi^4} \left( -\frac{2}{\epsilon} + \gamma - \ln \pi + \ln \frac{m_\pi^2}{\mu^2} - \frac{4}{3} \right) . \quad (2.15)$$

where the parameter  $\epsilon \rightarrow 0^+$ ,  $\gamma$  is the Euler-Mascheroni constant, and  $\mu$  is the renormalization scale brought in by the dimensional regularization procedure. The isospin structure  $\boldsymbol{\tau}_1 \cdot \boldsymbol{\tau}_2$  multiplying the polynomial  $P_2(k)$  can be reduced by Fierz rearrangement so as to match structures occurring in the LO  $v^{\text{CT0}}$  and N<sup>2</sup>LO  $v^{\text{CT2}}(\mathbf{k})$  contact contributions. Indeed, because of the antisymmetry of two-nucleon states,

$$\boldsymbol{\tau}_1 \cdot \boldsymbol{\tau}_2 = -2 - \boldsymbol{\sigma}_1 \cdot \boldsymbol{\sigma}_2 , \quad (2.16)$$

$$\boldsymbol{\tau}_1 \cdot \boldsymbol{\tau}_2 k^2 = -4 (1 + \boldsymbol{\sigma}_1 \cdot \boldsymbol{\sigma}_2) K^2 - k^2 . \quad (2.17)$$

It is then seen that the terms in  $P_0$  and  $P_2(k)$  renormalize  $C_S$ ,  $C_T$ ,  $C_1$ ,  $C_2$ ,  $C_4$  and  $C_6$ . For example, the last term of Eq. (2.11) is absorbed by the redefinition,

$$C_6 = \overline{C}_6 + \frac{3g_A^4}{8\pi^2 F_\pi^4} \mu^{-\epsilon} \left( -\frac{2}{\epsilon} + \gamma - \ln \pi + \ln \frac{m_\pi^2}{\mu^2} - \frac{4}{3} \right), \quad (2.18)$$

where the factor  $\mu^{-\epsilon}$  is needed because the mass dimension of the LEC  $C_6$  is  $d-7$  in  $d$  space dimensions. Note that the renormalized  $\overline{C}_6$  remains  $\mu$ -independent, as becomes obvious by taking the logarithmic derivative with respect to  $\mu$  and neglecting  $O(\epsilon)$  terms. For ease of notation, we will omit the overline and tacitly imply that the LECs have been properly renormalized.

The contributions in Eqs. (2.7), (2.9), and (2.8) lead to further renormalization of the LEC's  $C_S$  and  $C_T$ , as well as the axial coupling constant  $g_A$  entering the LO OPE:

$$v_g + v_i = \frac{4g_A^2}{3F_\pi^2} C_T \boldsymbol{\tau}_1 \cdot \boldsymbol{\tau}_2 \boldsymbol{\sigma}_1 \cdot \boldsymbol{\sigma}_2 M^{(3)} + \frac{g_A^2}{F_\pi^2} (3C_S - C_T \boldsymbol{\sigma}_1 \cdot \boldsymbol{\sigma}_2) M^{(3)}, \quad (2.19)$$

$$v_h(\mathbf{k}) = -\frac{g_A^4}{3F_\pi^4} \boldsymbol{\tau}_1 \cdot \boldsymbol{\tau}_2 \frac{\boldsymbol{\sigma}_1 \cdot \mathbf{k} \boldsymbol{\sigma}_2 \cdot \mathbf{k}}{\omega_k^2} M^{(3)}, \quad (2.20)$$

where the constants  $M^{(n)}$  are listed in Appendix B. The complete  $NN$  potential up to N<sup>2</sup>LO included is then given as

$$v(\mathbf{k}, \mathbf{K}) = \overline{v}^{\text{CT0}} + \overline{v}^\pi(\mathbf{k}) + \overline{v}^{\text{CT2}}(\mathbf{k}, \mathbf{K}) + \overline{v}^{2\pi}(\mathbf{k}), \quad (2.21)$$

where  $\overline{v}^{\text{CT0}}$ ,  $\overline{v}^\pi$ ,  $\overline{v}^{\text{CT2}}$ , and  $\overline{v}^{2\pi}$  are defined in Eqs. (2.2), (2.3), (2.4), and (2.12), respectively, and the overline indicates that the LEC's  $g_A$  and some of the  $C'_i$  have been renormalized.

### III. ELECTROMAGNETIC CURRENTS

In this section we construct the electromagnetic current operator for a two-nucleon system in  $\chi\text{EFT}$ . In the power-counting scheme of Ref. [7], the LO term results from the coupling of the external photon field to the individual nucleons, and is counted as  $eQ^{-2}$ , where a factor  $eQ$  is from the  $\gamma NN$  vertex, and a factor  $Q^{-3}$  follows from the momentum  $\delta$ -function implicit in this type of disconnected diagrams, see panel a) of Fig. 2. Higher order terms are suppressed by additional powers of  $Q$ , and formal expressions up to N<sup>3</sup>LO, *i.e.*  $eQ$ , have been derived in Ref. [7]. In this section, we proceed to regularize the loop integrals entering these N<sup>3</sup>LO currents, and to derive the corresponding finite parts.

At this order, we distinguish among four classes of contributions: i) currents generated by minimal substitution in the four-nucleon contact interactions involving two gradients of the nucleons' fields, as well as by non-minimal couplings (these were not considered in Ref. [7]); ii) two-pion exchange currents at one loop; iii) one-loop corrections to tree-level currents; and iv)  $(Q/M)^2$  relativistic corrections to the NLO currents resulting from the non-relativistic reduction of the vertices. The latter are neglected in the present work.

For completeness, we report below the expressions up to N<sup>2</sup>LO derived in Ref. [7], and shown in Fig. 2. As emphasized earlier, in the present study we do not explicitly include  $\Delta$ -isobar degrees of freedom. In the following, the momenta are defined as

$$\mathbf{k}_i = \mathbf{p}'_i - \mathbf{p}_i, \quad \mathbf{K}_i = (\mathbf{p}'_i + \mathbf{p}_i)/2, \quad (3.1)$$



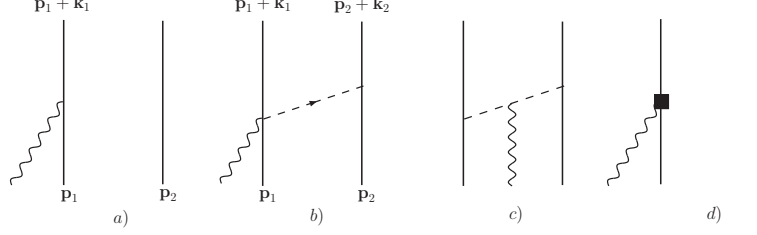


FIG. 2: Diagrams illustrating one- and two-body currents entering at LO ( $eQ^{-2}$ ), panel a), NLO ( $eQ^{-1}$ ), panels b) and c), and N<sup>2</sup>LO ( $eQ^0$ ), panel d). Nucleons, pions, and photons are denoted by solid, dashed, and wavy lines, respectively. The square represents the  $(Q/m_N)^2$  relativistic correction to the LO one-body current. Only one among the possible time orderings is shown for the NLO currents.

where  $\mathbf{p}_i$  and  $\mathbf{p}'_i$  are the initial and final momenta of nucleon  $i$ .

The LO contribution of panel a) in Fig. 2 is

$$\mathbf{j}_a^{\text{LO}} = \frac{e}{2m_N} \left[ 2e_{N,1} \mathbf{K}_1 + i\mu_{N,1} \boldsymbol{\sigma}_1 \times \mathbf{q} \right] + 1 \rightleftharpoons 2, \quad (3.2)$$

where  $\mathbf{q}$  is the photon momentum,  $\mathbf{q} = \mathbf{k}_i$ , and

$$e_N = (1 + \tau_z)/2, \quad \kappa_N = (\kappa_S + \kappa_V \tau_z)/2, \quad \mu_N = e_N + \kappa_N, \quad (3.3)$$

$\kappa_S$  and  $\kappa_V$  being the isoscalar and isovector combinations of the anomalous magnetic moments of the proton and neutron ( $\kappa_S = -0.12 \mu_N$  and  $\kappa_V = 3.706 \mu_N$ ). Loop corrections to the one-body current above, occurring at NLO and N<sup>2</sup>LO, are absorbed into  $\kappa_S$  and  $\kappa_V$ . The NLO seagull and pion-in-flight contributions, represented in panels b) and c), are:

$$\mathbf{j}_b^{\text{NLO}} = -ie \frac{g_A^2}{F_\pi^2} (\boldsymbol{\tau}_1 \times \boldsymbol{\tau}_2)_z \boldsymbol{\sigma}_1 \frac{\boldsymbol{\sigma}_2 \cdot \mathbf{k}_2}{\omega_{k_2}^2} + 1 \rightleftharpoons 2, \quad (3.4)$$

$$\mathbf{j}_c^{\text{NLO}} = ie \frac{g_A^2}{F_\pi^2} (\boldsymbol{\tau}_1 \times \boldsymbol{\tau}_2)_z \frac{\mathbf{k}_1 - \mathbf{k}_2}{\omega_{k_1}^2 \omega_{k_2}^2} \boldsymbol{\sigma}_1 \cdot \mathbf{k}_1 \boldsymbol{\sigma}_2 \cdot \mathbf{k}_2, \quad (3.5)$$

where the momenta transferred to nucleons 1 and 2 add up to  $\mathbf{q}$ ,  $\mathbf{k}_1 + \mathbf{k}_2 = \mathbf{q}$ . Lastly, the N<sup>2</sup>LO (relativistic) correction to the LO current, represented in panel d), reads:

$$\begin{aligned} \mathbf{j}_d^{\text{N}^2\text{LO}} = & - \frac{e}{8m_N^3} e_{N,1} \left[ 2 \left( K_1^2 + q^2/4 \right) (2\mathbf{K}_1 + i\boldsymbol{\sigma}_1 \times \mathbf{q}) + \mathbf{K}_1 \cdot \mathbf{q} (\mathbf{q} + 2i\boldsymbol{\sigma}_1 \times \mathbf{K}_1) \right] \\ & - \frac{ie}{8m_N^3} \kappa_{N,1} \left[ \mathbf{K}_1 \cdot \mathbf{q} (4\boldsymbol{\sigma}_1 \times \mathbf{K}_1 - i\mathbf{q}) - (2i\mathbf{K}_1 - \boldsymbol{\sigma}_1 \times \mathbf{q}) q^2/2 \right. \\ & \left. + 2(\mathbf{K}_1 \times \mathbf{q}) \boldsymbol{\sigma}_1 \cdot \mathbf{K}_1 \right] + 1 \rightleftharpoons 2. \end{aligned} \quad (3.6)$$

In addition to the classes mentioned earlier, there are N<sup>3</sup>LO contributions [24] involving the standard  $\pi NN$  vertex on one nucleon, and  $\gamma\pi NN$  vertices of order  $eQ^2$  on the other nucleon, derived from the following interaction Hamiltonian [25]

$$\begin{aligned} H_{\gamma\pi NN}^{(2)} = & \frac{e}{F_\pi} \int d\mathbf{x} N^\dagger(\mathbf{x}) \left[ d'_8 \nabla \pi_z(\mathbf{x}) + d'_9 \tau_a \nabla \pi_a(\mathbf{x}) \right. \\ & \left. - d'_{21} \epsilon_{zab} \tau_a \boldsymbol{\sigma} \times \nabla \pi_b(\mathbf{x}) \right] N(\mathbf{x}) \cdot \nabla \times \mathbf{A}(\mathbf{x}), \end{aligned} \quad (3.7)$$

where the notation and conventions of Ref. [7] have been adopted for the nucleon ( $N$ ), pion ( $\pi_a$ ), and photon ( $\mathbf{A}$ ) fields, and  $d'_8$ ,  $d'_9$ , and  $d'_{21}$  are related to the original couplings given by Fettes *et al.* [25] via  $d'_8 = 8[d_8 + g_A/(64 m_N^2)]$  and similarly for  $d'_9$ , and  $d'_{21} = 2 d_{21} + d_{22}$ . The resulting two-body current is given by

$$\mathbf{j}_{\text{tree}}^{\text{N}^3\text{LO}} = i e \frac{g_A}{F_\pi^2} \left[ (d'_8 \tau_{2,z} + d'_9 \boldsymbol{\tau}_1 \cdot \boldsymbol{\tau}_2) \mathbf{k}_2 - d'_{21} (\boldsymbol{\tau}_1 \times \boldsymbol{\tau}_2)_z \boldsymbol{\sigma}_1 \times \mathbf{k}_2 \right] \times \mathbf{q} \frac{\boldsymbol{\sigma}_2 \cdot \mathbf{k}_2}{\omega_{k_2}^2} + 1 \rightleftharpoons 2, \quad (3.8)$$

and in principle the unknown LEC's  $d'_8$ ,  $d'_9$ , and  $d'_{21}$  could be determined by pion photo-production data on a single nucleon or nuclear data (as discussed in Sec. I). The isovector part of  $\mathbf{j}_{\text{tree}}^{\text{N}^3\text{LO}}$  has the same structure as the current involving  $N$ - $\Delta$  excitation [7], to which it reduces if the following identifications are made:  $d'_{21}/d'_8 = 1/4$ , and  $d'_8 = 4 \mu^* h_A / (9 m_N \Delta)$ , where  $h_A$  is the  $\pi N \Delta$  coupling constant,  $\mu^*$  is the  $N \Delta$ -transition magnetic moment, and  $\Delta$  is the  $\Delta$ - $N$  mass difference,  $\Delta = m_\Delta - m_N$ .

Configuration-space representations of the current operators follow from

$$\mathbf{j}^{(1)}(\mathbf{q}) = \int_{\mathbf{k}_1} \int_{\mathbf{K}_1} e^{i\mathbf{k}_1 \cdot (\mathbf{r}'_1 + \mathbf{r}_1)/2} e^{i\mathbf{K}_1 \cdot (\mathbf{r}'_1 - \mathbf{r}_1)} \bar{\delta}(\mathbf{k}_1 - \mathbf{q}) \mathbf{j}^{(1)}(\mathbf{k}_1, \mathbf{K}_1), \quad (3.9)$$

$$\begin{aligned} \mathbf{j}^{(2)}(\mathbf{q}) &= \int_{\mathbf{k}_1} \int_{\mathbf{k}_2} e^{i\mathbf{k}_1 \cdot \mathbf{r}_1} e^{i\mathbf{k}_2 \cdot \mathbf{r}_2} \bar{\delta}(\mathbf{k}_1 + \mathbf{k}_2 - \mathbf{q}) \mathbf{j}^{(2)}(\mathbf{k}_1, \mathbf{k}_2) \\ &= e^{i\mathbf{q} \cdot \mathbf{R}} \int_{\mathbf{k}} e^{i\mathbf{k} \cdot \mathbf{r}} \mathbf{j}^{(2)}(\mathbf{q}, \mathbf{k}), \end{aligned} \quad (3.10)$$

where  $\mathbf{j}^{(1)}$  or  $\mathbf{j}^{(2)}$  denote any one-body or two-body operators, respectively, and  $\bar{\delta}(\dots) \equiv (2\pi)^3 \delta(\dots)$ . Note that  $\mathbf{K}_i \rightarrow -i \nabla'_i \delta(\mathbf{r}'_i - \mathbf{r}_i)$ , *i.e.* the configuration-space representation of the momentum operator, and in the second line of Eq. (3.10)  $\mathbf{R}$  and  $\mathbf{r}$  are the center-of-mass and relative positions of the two nucleons.

### A. $\text{N}^3\text{LO}$ currents: terms from four-nucleon contact interactions

The  $\text{N}^3\text{LO}$  currents obtained by minimal substitution in the contact interactions involving two gradients of the nucleons' fields have been constructed in Ref. [7], and are reported below for reference:

$$\begin{aligned} \mathbf{j}_{\text{CT}\gamma}^{\text{N}^3\text{LO}} &= -e e_1 \left[ 2 (2 C'_1 - C'_2) \mathbf{K}_2 + 4 C'_3 \mathbf{K}_1 + i C'_4 (\boldsymbol{\sigma}_1 + \boldsymbol{\sigma}_2) \times \mathbf{k}_2 + i C'_5 \boldsymbol{\sigma}_1 \times \mathbf{k}_1 \right. \\ &\quad - i C'_6 \boldsymbol{\sigma}_2 \times \mathbf{k}_1 + 2 (2 C'_7 - C'_{10}) (\mathbf{K}_2 \cdot \boldsymbol{\sigma}_2) \boldsymbol{\sigma}_1 + 2 (2 C'_8 - C'_{11}) (\mathbf{K}_2 \cdot \boldsymbol{\sigma}_1) \boldsymbol{\sigma}_2 \\ &\quad - 2 C'_{13} [(\mathbf{K}_1 \cdot \boldsymbol{\sigma}_1) \boldsymbol{\sigma}_2 + (\mathbf{K}_1 \cdot \boldsymbol{\sigma}_2) \boldsymbol{\sigma}_1] + 2 (2 C'_9 - C'_{12}) \mathbf{K}_2 (\boldsymbol{\sigma}_1 \cdot \boldsymbol{\sigma}_2) \\ &\quad \left. - 4 C'_{14} \mathbf{K}_1 (\boldsymbol{\sigma}_1 \cdot \boldsymbol{\sigma}_2) \right] + 1 \rightleftharpoons 2. \end{aligned} \quad (3.11)$$

In addition to these, there are contributions due to non-minimal couplings, as derived in Appendix A,

$$\mathbf{j}_{\text{CT}\gamma\text{nm}}^{\text{N}^3\text{LO}} = -i e \left[ C'_{15} \boldsymbol{\sigma}_1 + C'_{16} (\tau_{1,z} - \tau_{2,z}) \boldsymbol{\sigma}_1 \right] \times \mathbf{q} + 1 \rightleftharpoons 2. \quad (3.12)$$

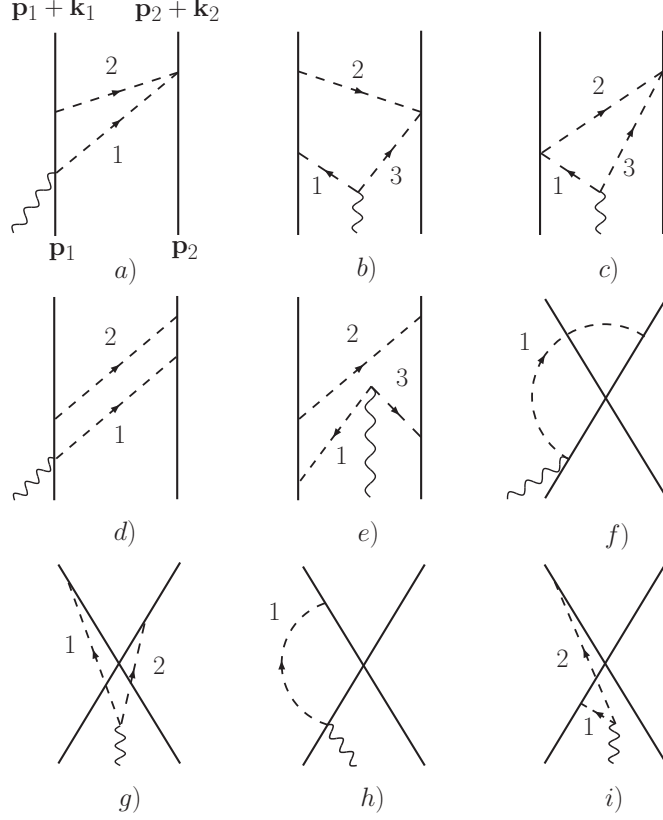


FIG. 3: Diagrams illustrating one-loop two-body currents entering at  $N^3\text{LO}$  ( $eQ$ ), notation as in Fig. 2. Only one among the possible time orderings is shown for each contribution.

### B. $N^3\text{LO}$ currents: one-loop corrections

Loop corrections entering at  $N^3\text{LO}$  have been derived in Ref. [7], and their formal expressions, corrected from a number of typographical errors, are listed, for reference, in Appendix C of the present paper. In Ref. [7], it was also shown that the one-loop currents satisfy the continuity equation with the two-pion-exchange potential of Sec. II A. Here we discuss their renormalization. We start off by considering the currents (involving one and two pions) illustrated in panels a), d), f), g), h), and i) of Fig. 3. Those in panels b), c), and e) (involving three pions) are discussed in Sec. IV and Appendix D, since for them we only derive the magnetic dipole operators. In terms of the kernels defined in Appendix B, we obtain:

$$\mathbf{j}_a^{\text{N}^3\text{LO}} = -ie \frac{g_A^2}{F_\pi^4} I^{(0)}(k_2) \left[ 2 \tau_{2,z} \boldsymbol{\sigma}_1 \times \mathbf{k}_2 + (\boldsymbol{\tau}_1 \times \boldsymbol{\tau}_2)_z \mathbf{k}_2 \right] + 1 \rightleftharpoons 2, \quad (3.13)$$

$$\begin{aligned} \mathbf{j}_d^{\text{N}^3\text{LO}} = & -ie \frac{g_A^4}{F_\pi^4} \left[ \left[ k_2^2 J^{(0)}(k_2) - J^{(2)}(k_2) \right] \left[ 2 \tau_{2,z} \boldsymbol{\sigma}_1 \times \mathbf{k}_2 + (\boldsymbol{\tau}_1 \times \boldsymbol{\tau}_2)_z \mathbf{k}_2 \right] \right. \\ & \left. + 4 \tau_{1,z} J_{ij}^{(2)}(k_2) (\boldsymbol{\sigma}_2 \times \mathbf{k}_2)_j \right] + 1 \rightleftharpoons 2, \end{aligned} \quad (3.14)$$

$$\mathbf{j}_g^{\text{N}^3\text{LO}} = -2ie \frac{g_A^2}{F_\pi^2} C_T (\boldsymbol{\tau}_1 \times \boldsymbol{\tau}_2)_z J_{ij}^{(2)}(q) \sigma_{1,j} \boldsymbol{\sigma}_2 \cdot \mathbf{q} + 1 \rightleftharpoons 2, \quad (3.15)$$

$$\mathbf{j}_i^{\text{N}^3\text{LO}} = -2ie \frac{g_A^2}{F_\pi^2} \tau_{1,z} J_{ij}^{(2)}(q) [C_S (\boldsymbol{\sigma}_1 \times \mathbf{q})_j - C_T (\boldsymbol{\sigma}_2 \times \mathbf{q})_j] + 1 \rightleftharpoons 2, \quad (3.16)$$

and the currents in panels f) and h) vanish in the static limit [7]. Insertion of the finite parts of the various kernels in the expressions above then gives

$$\bar{\mathbf{j}}_a^{\text{N}^3\text{LO}} = ie \frac{g_A^2}{8\pi^2 F_\pi^4} G(k_2) [2\tau_{2,z} \boldsymbol{\sigma}_1 \times \mathbf{k}_2 + (\boldsymbol{\tau}_1 \times \boldsymbol{\tau}_2)_z \mathbf{k}_2] + 1 \rightleftharpoons 2, \quad (3.17)$$

$$\begin{aligned} \bar{\mathbf{j}}_d^{\text{N}^3\text{LO}} = & -ie \frac{g_A^4}{8\pi^2 F_\pi^4} G(k_2) \left[ \left( 3 - \frac{4m_\pi^2}{4m_\pi^2 + k_2^2} \right) [2\tau_{2,z} \boldsymbol{\sigma}_1 \times \mathbf{k}_2 + (\boldsymbol{\tau}_1 \times \boldsymbol{\tau}_2)_z \mathbf{k}_2] \right. \\ & \left. - 4\tau_{1,z} \boldsymbol{\sigma}_2 \times \mathbf{k}_2 \right] + 1 \rightleftharpoons 2, \end{aligned} \quad (3.18)$$

$$\bar{\mathbf{j}}_g^{\text{N}^3\text{LO}} = ie \frac{g_A^2 C_T}{4\pi^2 F_\pi^2} (\boldsymbol{\tau}_1 \times \boldsymbol{\tau}_2)_z G(q) \boldsymbol{\sigma}_1 \boldsymbol{\sigma}_2 \cdot \mathbf{q} + 1 \rightleftharpoons 2, \quad (3.19)$$

$$\bar{\mathbf{j}}_i^{\text{N}^3\text{LO}} = ie \frac{g_A^2}{4\pi^2 F_\pi^2} \tau_{1,z} G(q) (C_S \boldsymbol{\sigma}_1 \times \mathbf{q} - C_T \boldsymbol{\sigma}_2 \times \mathbf{q}) + 1 \rightleftharpoons 2, \quad (3.20)$$

and the loop function  $G$  is defined in Eq. (2.13). The divergent parts of the kernels lead to renormalization of some of the LEC's  $C'_i$ . They are given by

$$\mathbf{j}_{\infty,a}^{\text{N}^3\text{LO}} = ie \frac{g_A^2}{8\pi^2 F_\pi^4} \left( \frac{2}{\epsilon} + \dots \right) [-2\tau_{2,z} \boldsymbol{\sigma}_1 \times \mathbf{k}_2 - (\boldsymbol{\tau}_1 \times \boldsymbol{\tau}_2)_z \mathbf{k}_2] + 1 \rightleftharpoons 2, \quad (3.21)$$

$$\mathbf{j}_{\infty,b}^{\text{N}^3\text{LO}} = ie \frac{g_A^2}{8\pi^2 F_\pi^4} \left( \frac{2}{\epsilon} + \dots \right) \left[ 2\tau_{2,z} \boldsymbol{\sigma}_1 \times (\mathbf{k}_2 - \mathbf{q}) - \frac{2}{3} (\boldsymbol{\tau}_1 \times \boldsymbol{\tau}_2)_z \mathbf{k}_2 \right] + 1 \rightleftharpoons 2, \quad (3.22)$$

$$\mathbf{j}_{\infty,c}^{\text{N}^3\text{LO}} = ie \frac{1}{48\pi^2 F_\pi^4} \left( \frac{2}{\epsilon} + \dots \right) (\boldsymbol{\tau}_1 \times \boldsymbol{\tau}_2)_z (\mathbf{k}_1 - \mathbf{k}_2), \quad (3.23)$$

$$\mathbf{j}_{\infty,d}^{\text{N}^3\text{LO}} = ie \frac{g_A^4}{8\pi^2 F_\pi^4} \left( \frac{2}{\epsilon} + \dots \right) [\tau_{2,z} \boldsymbol{\sigma}_1 \times (6\mathbf{k}_2 - 4\mathbf{k}_1) + 3(\boldsymbol{\tau}_1 \times \boldsymbol{\tau}_2)_z \mathbf{k}_2] + 1 \rightleftharpoons 2, \quad (3.24)$$

$$\mathbf{j}_{\infty,e}^{\text{N}^3\text{LO}} = ie \frac{g_A^4}{8\pi^2 F_\pi^4} \left( \frac{2}{\epsilon} + \dots \right) \left[ 10\tau_{2,z} \boldsymbol{\sigma}_1 \times \mathbf{k}_1 + \frac{5}{6} (\boldsymbol{\tau}_1 \times \boldsymbol{\tau}_2)_z \mathbf{k}_2 \right] + 1 \rightleftharpoons 2, \quad (3.25)$$

$$\mathbf{j}_{\infty,g}^{\text{N}^3\text{LO}} = ie \frac{g_A^2}{4\pi^2 F_\pi^2} \left( \frac{2}{\epsilon} + \dots \right) (\boldsymbol{\tau}_1 \times \boldsymbol{\tau}_2)_z C_T [\boldsymbol{\sigma}_2 \boldsymbol{\sigma}_1 \cdot \mathbf{q} - \boldsymbol{\sigma}_1 \boldsymbol{\sigma}_2 \cdot \mathbf{q}], \quad (3.26)$$

$$\mathbf{j}_{\infty,i}^{\text{N}^3\text{LO}} = ie \frac{g_A^2}{4\pi^2 F_\pi^2} \left( \frac{2}{\epsilon} + \dots \right) \tau_{1,z} [C_T \boldsymbol{\sigma}_2 \times \mathbf{q} - C_S \boldsymbol{\sigma}_1 \times \mathbf{q}] + 1 \rightleftharpoons 2, \quad (3.27)$$

where the dots denote finite contributions depending on the renormalization point. When combined together, all these divergencies can be absorbed by the renormalization of the  $C'_i$ , which is not the case for the individual contributions. For instance, taking into account the antisymmetry properties of nucleons,

$$\begin{aligned} (\tau_{2,z} \boldsymbol{\sigma}_1 + \tau_{1,z} \boldsymbol{\sigma}_2) \times \mathbf{q} &= -(\tau_{1,z} \boldsymbol{\sigma}_1 + \tau_{2,z} \boldsymbol{\sigma}_2) \times \mathbf{q} \\ &= \frac{1}{2} (\boldsymbol{\tau}_1 \times \boldsymbol{\tau}_2)_z [\boldsymbol{\sigma}_1 \boldsymbol{\sigma}_2 \cdot \mathbf{q} - \boldsymbol{\sigma}_2 \boldsymbol{\sigma}_1 \cdot \mathbf{q}] \\ &= -\frac{1}{2} (\tau_{1,z} - \tau_{2,z}) (\boldsymbol{\sigma}_1 - \boldsymbol{\sigma}_2) \times \mathbf{q}, \end{aligned} \quad (3.28)$$

leading to renormalization of  $C'_{16}$ , and

$$(\boldsymbol{\tau}_1 \times \boldsymbol{\tau}_2)_z (\mathbf{k}_2 - \mathbf{k}_1) = -2 i e_1 (1 + \boldsymbol{\sigma}_1 \cdot \boldsymbol{\sigma}_2) (\mathbf{K}_1 - \mathbf{K}_2) + 1 \rightleftharpoons 2 , \quad (3.29)$$

leading to renormalization of  $C'_3$ ,  $C'_{14}$ ,  $(2 C'_1 - C'_2)$  and  $(2 C'_9 - C'_{12})$ .

### C. N<sup>3</sup>LO currents: one-loop corrections to tree-level currents

Contributions in this class are illustrated by the diagrams in Figs. 4 and 5. After including all possible time orderings, we find for those in Fig. 4:

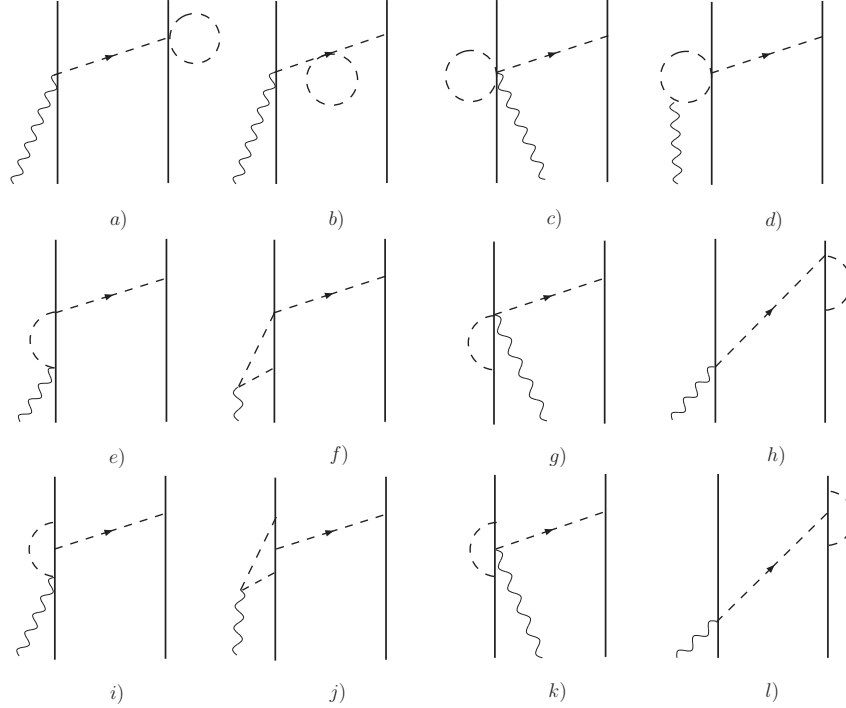


FIG. 4: Diagrams illustrating loop corrections to tree-level two-body currents, notation as in Fig. 2. Only one among the possible time orderings is shown for each contribution.

$$\text{type a)} = \mathbf{j}_b^{\text{NLO}} \left[ -\frac{3}{2 F_\pi^2} M^{(1)} \right] , \quad (3.30)$$

$$\text{type b)} = -i e \frac{g_A^2}{F_\pi^2} (\boldsymbol{\tau}_1 \times \boldsymbol{\tau}_2)_z \boldsymbol{\sigma}_1 \frac{\boldsymbol{\sigma}_2 \cdot \mathbf{k}_2}{\omega_{k_2}^2} \left[ -\frac{1}{\omega_{k_2}^2} \frac{m_\pi^2}{F_\pi^2} M^{(1)} \right] + 1 \rightleftharpoons 2 , \quad (3.31)$$

$$\text{type c)} = \mathbf{j}_b^{\text{NLO}} \left[ -\frac{5}{2 F_\pi^2} M^{(1)} \right] , \quad (3.32)$$

$$\text{type d)} = -i e \frac{g_A^2}{2 F_\pi^4} (\boldsymbol{\tau}_1 \times \boldsymbol{\tau}_2)_z I_{ij}^{(2)}(q) \sigma_{1,j} \frac{\boldsymbol{\sigma}_2 \cdot \mathbf{k}_2}{\omega_{k_2}^2} + 1 \rightleftharpoons 2 , \quad (3.33)$$

$$\text{type e)} = \mathbf{j}_b^{\text{NLO}} \left[ \frac{1}{F_\pi^2} M^{(1)} \right] , \quad (3.34)$$

$$\text{type f)} = i e \frac{g_A^2}{2 F_\pi^4} (\boldsymbol{\tau}_1 \times \boldsymbol{\tau}_2)_z I_{ij}^{(2)}(q) \sigma_{1,j} \frac{\boldsymbol{\sigma}_2 \cdot \mathbf{k}_2}{\omega_{k_2}^2} + 1 \rightleftharpoons 2 , \quad (3.35)$$

$$\text{type j)} = i e \frac{2 g_A^4}{F_\pi^4} \tau_{2,z} J_{ij}^{(2)}(q) (\mathbf{k}_2 \times \mathbf{q})_j \frac{\boldsymbol{\sigma}_2 \cdot \mathbf{k}_2}{\omega_{k_2}^2} + 1 \rightleftharpoons 2 , \quad (3.36)$$

$$\text{type k)} = \text{type l)} = \mathbf{j}_b^{\text{NLO}} \left[ \frac{g_A^2}{6 F_\pi^2} M^{(3)} \right] , \quad (3.37)$$

while for those in Fig. 5:

$$\text{type m)} + \text{type n)} = \mathbf{j}_c^{\text{NLO}} \left[ -\frac{3}{F_\pi^2} M^{(1)} \right] , \quad (3.38)$$

$$\text{type o)} + \text{type p)} = \mathbf{j}_c^{\text{NLO}} \left( -\frac{1}{\omega_{k_1}^2} - \frac{1}{\omega_{k_2}^2} \right) \frac{m_\pi^2}{F_\pi^2} M^{(1)} , \quad (3.39)$$

$$\text{type q)} = \mathbf{j}_c^{\text{NLO}} \left[ -\frac{5}{F_\pi^2} M^{(1)} \right] , \quad (3.40)$$

$$\text{type r)} = i e \frac{g_A^2}{F_\pi^4} (\boldsymbol{\tau}_1 \times \boldsymbol{\tau}_2)_z I_{ij}^{(2)}(q) (\mathbf{k}_1 - \mathbf{k}_2)_j \frac{\boldsymbol{\sigma}_1 \cdot \mathbf{k}_1}{\omega_{k_1}^2} \frac{\boldsymbol{\sigma}_2 \cdot \mathbf{k}_2}{\omega_{k_2}^2} , \quad (3.41)$$

$$\text{type u)} + \text{type v)} = \mathbf{j}_c^{\text{NLO}} \left[ \frac{g_A^2}{3 F_\pi^2} M^{(3)} \right] , \quad (3.42)$$

where  $\mathbf{j}_b^{\text{NLO}}$  and  $\mathbf{j}_c^{\text{NLO}}$  are the seagull and pion-in-flight currents of Eqs. (3.4) and (3.5), and the constants  $M^{(n)}$ , and kernels  $I_{ij}^{(2)}(q)$  and  $J_{ij}^{(2)}(q)$  are given in Appendix B. The contributions associated with diagrams of type h), i), s), and t) vanish, since the integrand is an odd function of the loop momentum  $\mathbf{p}$ . Lastly, diagrams of type g) are of order  $e Q^2$  [7], and therefore beyond the order under consideration in the present study ( $e Q$ ), and only a subset of the irreducible diagrams is retained in the evaluation of the type j) contribution, see Appendix E.

A few comments are now in order. Firstly, the evaluation of the diagrams in the last row of Figs. 4 and 5 is carried out by including recoil corrections to the reducible diagrams of corresponding topology. Cancellations occur between the irreducible and these recoil-corrected reducible contributions. This is discussed in Appendix E.

Secondly, diagrams like those shown in Fig. 6 have not been considered since they are, like diagram g) in Fig. 4, of order  $e Q^2$ , as can be easily surmised by using the counting rules given in Ref. [7].

Thirdly, the contributions of type a), c), e), k)-l), m)-n), and u)-v) lead to (further) renormalization of  $g_A$ , while those of type b) and o)-p) renormalize the pion mass, namely  $\overline{m}_\pi^2 = m_\pi^2(1 + M^{(1)}/F_\pi^2)$ . Thus, both types are accounted for in the (renormalized) seagull and pion-in-flight currents. Diagrams j) and r) generate form-factor corrections—their finite parts follow from the  $I_{ij}^{(2)}$  and  $J_{ij}^{(2)}$  kernels—to the nucleon and pion electromagnetic couplings. However, the contributions of diagrams d) and f) exactly cancel out.

#### IV. MAGNETIC MOMENTS FROM PION EXCHANGES AT N<sup>3</sup>LO

To begin with, it is worthwhile making some general considerations. The magnetic moment operator  $\boldsymbol{\mu}$  due to a two-body current density  $\mathbf{J}(\mathbf{x})$  can be separated into a term

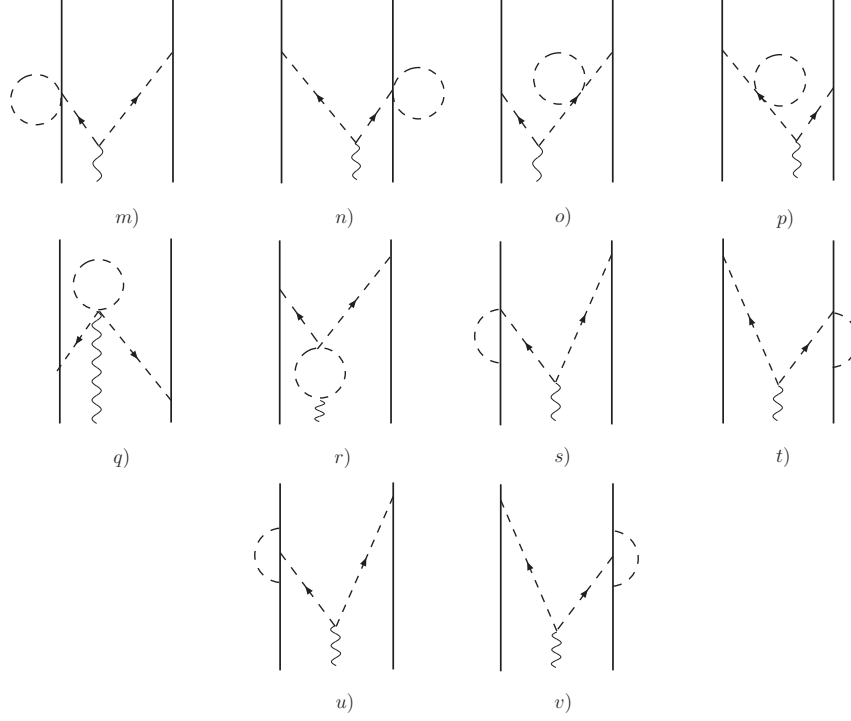


FIG. 5: Same as in Fig. 4.

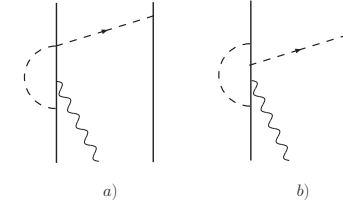


FIG. 6: Diagrams illustrating  $N^4\text{LO}$  ( $eQ^2$ ) loop corrections to tree-level currents not included in the present study, notation as in Fig. 2.

dependent on the center-of-mass position  $\mathbf{R}$  of the two particles and one independent of it [19], as

$$\boldsymbol{\mu}(\mathbf{R}, \mathbf{r}) = \frac{1}{2} \left[ \mathbf{R} \times \int d\mathbf{x} \mathbf{J}(\mathbf{x}) + \int d\mathbf{x} (\mathbf{x} - \mathbf{R}) \times \mathbf{J}(\mathbf{x}) \right], \quad (4.1)$$

where, because of translational invariance,  $\mathbf{J}(\mathbf{x})$  is actually a function of  $\mathbf{J}(\mathbf{x} - \mathbf{R}, \mathbf{r})$ ,  $\mathbf{r}$  being the relative position of the two particles, see Eq. (3.10). The first term in square brackets can be related via the continuity equation to the commutator of the charge density operator with the two-nucleon potential [19], assumed to be of the form  $\boldsymbol{\tau}_1 \cdot \boldsymbol{\tau}_2 V(\mathbf{r})$  but otherwise velocity independent (for example, the one- and two-pion-exchange potentials derived in Sec. II), while the second term can be written in terms of the Fourier transform of  $\mathbf{J}(\mathbf{x})$ , denoted by  $\mathbf{j}(\mathbf{q})$ . We find:

$$\boldsymbol{\mu}(\mathbf{R}, \mathbf{r}) = -\frac{1}{2} \left[ e (\boldsymbol{\tau}_1 \times \boldsymbol{\tau}_2)_z V(\mathbf{r}) \mathbf{R} \times \mathbf{r} + i \nabla_q \times \mathbf{j}(\mathbf{q})|_{\mathbf{q}=0} \right], \quad (4.2)$$

which, for our purposes, is more conveniently written in momentum space as

$$\boldsymbol{\mu}(\mathbf{R}, \mathbf{k}) = -\frac{i}{2} \left[ e (\boldsymbol{\tau}_1 \times \boldsymbol{\tau}_2)_z \mathbf{R} \times \nabla_{\mathbf{k}} v(\mathbf{k}) + \nabla_{\mathbf{q}} \times \mathbf{j}(\mathbf{q}, \mathbf{k})|_{\mathbf{q}=0} \right], \quad (4.3)$$

where  $v(\mathbf{k})$  denotes the Fourier transform of  $V(\mathbf{r})$ . The first term above is Sachs' contribution [20], denoted as  $\boldsymbol{\mu}_{\text{Sachs}}$ , to the magnetic moment: it is uniquely determined by the potential between the two nucleons.

Therefore, the currents a)-e) in Fig. 3 generate a Sachs' magnetic moment—currents g) and i) do not contribute to it—given by

$$\bar{\boldsymbol{\mu}}_{\text{Sachs}}^{\text{N}^3\text{LO}}(\mathbf{R}, \mathbf{k}) = -\frac{i}{2} e (\boldsymbol{\tau}_1 \times \boldsymbol{\tau}_2)_z \mathbf{R} \times \nabla_{\mathbf{k}} \bar{v}_0^{2\pi}(k), \quad (4.4)$$

where  $\bar{v}_0^{2\pi}(k)$  is the term proportional to  $\boldsymbol{\tau}_1 \cdot \boldsymbol{\tau}_2$  in Eq. (2.12), *i.e.*

$$\bar{v}_0^{2\pi}(k) = \frac{1}{48\pi^2 F_\pi^4} G(k) \left[ 4m_\pi^2(1 + 4g_A^2 - 5g_A^4) + k^2(1 + 10g_A^2 - 23g_A^4) - \frac{48g_A^4 m_\pi^4}{4m_\pi^2 + k^2} \right]. \quad (4.5)$$

The relation (4.4) can easily be verified by direct evaluation of  $(\mathbf{R}/2) \times \mathbf{j}_{a-e}(\mathbf{q} = 0, \mathbf{k})$ . The currents a)-e) and i) also generate a translationally invariant contribution, namely the second term in Eq. (4.3), which reads (see Appendix D for details)

$$\bar{\boldsymbol{\mu}}^{\text{N}^3\text{LO}}(\mathbf{k}) = \frac{e g_A^2}{8\pi^2 F_\pi^4} \tau_{2,z} \left[ F_0(k) \boldsymbol{\sigma}_1 - F_2(k) \frac{\mathbf{k} \boldsymbol{\sigma}_1 \cdot \mathbf{k}}{k^2} \right] + \frac{e g_A^2}{2\pi^2 F_\pi^2} \tau_{2,z} (C_S \boldsymbol{\sigma}_2 - C_T \boldsymbol{\sigma}_1) + 1 \rightleftharpoons 2, \quad (4.6)$$

where the functions  $F_i(k)$  are

$$F_0(k) = 1 - 2g_A^2 + \frac{8g_A^2 m_\pi^2}{k^2 + 4m_\pi^2} + G(k) \left[ 2 - 2g_A^2 - \frac{4(1 + g_A^2) m_\pi^2}{k^2 + 4m_\pi^2} + \frac{16g_A^2 m_\pi^4}{(k^2 + 4m_\pi^2)^2} \right], \quad (4.7)$$

$$F_2(k) = 2 - 6g_A^2 + \frac{8g_A^2 m_\pi^2}{k^2 + 4m_\pi^2} + G(k) \left[ 4g_A^2 - \frac{4(1 + 3g_A^2) m_\pi^2}{k^2 + 4m_\pi^2} + \frac{16g_A^2 m_\pi^4}{(k^2 + 4m_\pi^2)^2} \right]. \quad (4.8)$$

It is interesting to note that the constant  $2 - 6g_A^2$  in  $F_2(k)$  would lead to a long-range contribution of the type  $[\tau_{2,z}(\boldsymbol{\sigma}_1 \cdot \nabla) \nabla + 1 \rightleftharpoons 2] 1/r$  in the magnetic moment, which is, however, fictitious in the present context of an effective field theory valid at low momenta—in performing the Fourier transform, the high momentum components are suppressed by the cutoff  $C_\Lambda(k)$ .

We now compare the magnetic moment operator derived here with that obtained in Ref. [5]. Firstly, we note that the Sachs term is ignored in that work. Of course, it vanishes in two-body systems because of its dependence on  $\mathbf{R}$ . However, in  $A > 2$  systems the center-of-mass position of a nucleon pair will not generally coincide with that of the nucleus, and therefore this term will contribute.

Secondly, the treatment of the box diagrams, panels d) and e) in Fig. 3, is different in our approach, since the expressions listed in Eqs. (D2) and (D7) result from combining recoil-corrected reducible *and* irreducible diagrams. In particular, had we retained *only* the latter, the isospin structure of  $\boldsymbol{\mu}_d^{\text{N}^3\text{LO}}(\mathbf{k}) + \boldsymbol{\mu}_e^{\text{N}^3\text{LO}}(\mathbf{k})$  would have contained, in addition to terms proportional to  $\tau_{i,z}$ , also the term proportional to  $(\boldsymbol{\tau}_1 \times \boldsymbol{\tau}_2)_z$  present in Eq. (46) of Ref. [5].

Lastly, we find that type a) and b) contributions in Fig. 3, which only consist of irreducible diagrams, are in agreement with the corresponding terms in Eq. (46) of Ref. [5]. This is



easily seen by considering the Fourier transform of that equation. To this end, we first observe that

$$\int_0^1 dz \ln [1 + z(z-1)p^2/m_\pi^2] = G(p) - 2 , \quad (4.9)$$

and then note that

$$\int d\mathbf{r} e^{-i\mathbf{k}\cdot\mathbf{r}} \left[ r \frac{d}{dr} \int_{\mathbf{p}} e^{i\mathbf{p}\cdot\mathbf{r}} [2 - G(p)] \right] = 3 G(k) + k G'(k) - 6 , \quad (4.10)$$

$$\int d\mathbf{r} e^{-i\mathbf{k}\cdot\mathbf{r}} \left[ \hat{\mathbf{r}} \boldsymbol{\sigma} \cdot \hat{\mathbf{r}} r \frac{d}{dr} \int_{\mathbf{p}} e^{i\mathbf{p}\cdot\mathbf{r}} [2 - G(p)] \right] = [G(k) - 2] \boldsymbol{\sigma} + k G'(k) \frac{\mathbf{k} \boldsymbol{\sigma} \cdot \mathbf{k}}{k^2} , \quad (4.11)$$

where  $G'(k)$  denotes the derivative of  $G(k)$ . Inserting these relations into Eq. (46) leads to a similar Eq. (4.6), but with  $C_S$  and  $C_T$  taken to be zero, and

$$F_0(k) \rightarrow G(k) \left( 2 - \frac{4 m_\pi^2}{k^2 + 4 m_\pi^2} \right) - 2 ,$$

$$F_2(k) \rightarrow 2 - G(k) \frac{4 m_\pi^2}{k^2 + 4 m_\pi^2} .$$

The  $F_2(k)$  above is the same as Eq. (4.8) (with  $g_A$  set to zero to remove the box contributions), while  $F_0(k)$  differs from Eq. (4.7) by a constant, which gives rise to a zero-ranged operator—operators of this type were dropped in Eq. (46) anyway.

To the magnetic moment operators of Eqs. (4.4) and (4.6), one has to add the term of one-pion range originating from the current  $\mathbf{j}_{\text{tree}}^{\text{N}^3\text{LO}}$  (Sec. III), given by

$$\overline{\boldsymbol{\mu}}_{\text{tree}}^{\text{N}^3\text{LO}} = e \frac{g_A}{F_\pi^2} \left[ (d'_8 \tau_{2,z} + d'_9 \boldsymbol{\tau}_1 \cdot \boldsymbol{\tau}_2) \mathbf{k} - d'_{21} (\boldsymbol{\tau}_1 \times \boldsymbol{\tau}_2)_z \boldsymbol{\sigma}_1 \times \mathbf{k} \right] \frac{\boldsymbol{\sigma}_2 \cdot \mathbf{k}}{k^2 + m_\pi^2} + 1 \rightleftharpoons 2 . \quad (4.12)$$

## V. DETERMINING THE LEC'S: FITTING THE $\text{N}^2\text{LO}$ $NN$ POTENTIAL

We find it convenient to formulate the  $NN$  scattering- and bound-state problems in momentum space [26]. In the case of scattering, we solve for the  $K$ -matrix

$$K_{L',L}^{JTS}(p',p) = v_{L',L}^{JTS}(p',p) + \frac{4\mu_N}{\pi} \int_0^\infty dk k^2 \sum_{L''} v_{L',L''}^{JTS}(p',k) \frac{\mathcal{P}}{p^2 - k^2} K_{L'',L}^{JTS}(k,p) , \quad (5.1)$$

where  $\mu_N$  is the reduced mass,  $\mathcal{P}$  denotes a principal-value integration, and the momentum-space matrix elements  $v_{L',L}^{JTS}(p',p)$  of the potential are defined as in Eqs. (3.3) and (3.4) of Ref. [17], but for the factor of  $2\pi$  in front of the integration over  $z = \hat{\mathbf{p}}' \cdot \hat{\mathbf{p}}$  being replaced here by  $1/(8\pi)$ , and the inclusion, in the present case, of an additional phase factor  $i^{L-L'}$ , which, for coupled channels, leads to mixing angles with signs conforming to the customary choice made in phase-shift analyses.

The integral equations above are discretized, and the resulting systems of linear equations are then solved by direct numerical inversion. The principal-value integration is removed by a standard subtraction technique [27]. Once the  $K$ -matrices in the various channels have been determined, the corresponding (on-shell)  $S$ -matrices are obtained from

$$S^{JTS}(p) = \left[ 1 + 2i \mu_N p K^{JTS}(p,p) \right]^{-1} \left[ 1 - 2i \mu_N p K^{JTS}(p,p) \right] , \quad (5.2)$$

TABLE I: Values for the nucleon axial coupling constant  $g_A$ , pion decay constant  $F_\pi$ , neutral and charged pion masses  $m_0$  and  $m_+$ , (twice)  $np$  reduced mass  $\mu_N$ , and  $\hbar c$ , used in the fits.

| $g_A$ | $F_\pi$ (MeV) | $m_0$ (MeV) | $m_+$ (MeV) | $2\mu_N$ (MeV) | $\hbar c$ (MeV-fm) |
|-------|---------------|-------------|-------------|----------------|--------------------|
| 1.29  | 184.8         | 134.9766    | 139.5702    | 938.9181       | 197.32696          |

from which phase shifts and, for coupled channels, mixing angles are easily determined [17].

The bound state (with  $JTS = 101$  and  $L, L' = 0, 2$ ) is obtained from solutions of the homogeneous integral equations [26]

$$w_L(p) = \frac{1}{E_d - p^2/(2\mu_N)} \frac{2}{\pi} \int_0^\infty dk k^2 \sum_{L'} v_{L,L'}^{101}(p, k) w_{L'}(k) , \quad (5.3)$$

and from these, for later reference, the configuration-space  $S$ - and  $D$ -wave components follow as

$$u_L(r) = \frac{2}{\pi} \int_0^\infty dp p^2 j_L(pr) w_L(p) . \quad (5.4)$$

Before turning our attention to a discussion of the phase-shift fits, we note that the potential constructed in Sec. II B needs to be (further) regularized because of its power-law behavior for large values of the momenta  $k$  and/or  $K$ . This is accomplished by including a high-momentum cutoff, which we take to be of the form

$$C_\Lambda(k, K) = e^{-(k^4 + 16K^4)/\Lambda^4} , \quad (5.5)$$

so that the matrix elements of the regularized potential entering the  $K$ -matrix and bound-state equations are obtained from

$$v^R(\mathbf{k}, \mathbf{K}) = v(\mathbf{k}, \mathbf{K}) C_\Lambda(k, K) , \quad (5.6)$$

and  $v(\mathbf{k}, \mathbf{K})$  is defined as in Eq. (2.21). In the following cutoff parameters  $\Lambda$  in the range 500–700 MeV are considered.

The LEC's  $C_S$ ,  $C_T$ , and  $C_i$ ,  $i = 1, \dots, 7$ , are determined by fitting the deuteron binding energy and  $S$ - and  $P$ -wave  $np$  phase shifts up to laboratory kinetic energies of 100 MeV, as obtained in the very recent (2008) analysis of Gross and Stadler [16]. The parameters characterizing the one- and two-pion exchange parts of the potential are listed in Table I, with the nucleon axial coupling constant  $g_A$  determined from the Golberger-Treiman relation  $g_A = g_{\pi NN} F_\pi / (2m_N)$ , where the  $\pi NN$  coupling constant is taken to have the value  $g_{\pi NN}^2 / (4\pi) = 13.63 \pm 0.20$  [28, 29]. In fact, in the OPE we include the isospin-symmetry breaking induced by the mass difference between charged and neutral pions, since it leads to significant effects in the  $^1S_0$  scattering length [30], and therefore the OPE potential reads

$$\bar{v}^\pi(\mathbf{k}) = -\frac{g_A^2}{3F_\pi^2} \left[ \boldsymbol{\tau}_1 \cdot \boldsymbol{\tau}_2 \left( \frac{1}{k^2 + m_0^2} + \frac{2}{k^2 + m_+^2} \right) + T_{12} \left( \frac{1}{k^2 + m_0^2} - \frac{1}{k^2 + m_+^2} \right) \right] \boldsymbol{\sigma}_1 \cdot \mathbf{k} \boldsymbol{\sigma}_2 \cdot \mathbf{k} , \quad (5.7)$$

where  $T_{12}$  is the isotensor operator defined as  $T_{12} = 3\tau_{1,z}\tau_{2,z} - \boldsymbol{\tau}_1 \cdot \boldsymbol{\tau}_2$ , and  $m_0$  and  $m_+$  are the neutral and charged pions masses. Finally, we note that the pion mass entering in the two-pion-exchange part is taken as  $m_\pi = (m_0 + 2m_+)/3$ .

The best-fit values obtained for the LEC's are listed in Table II for  $\Lambda=500$ , 600, and 700 MeV. The fitting strategy becomes obvious once the partial wave expansion of the potential

is carried out. In the case of spin-singlet ( $S = 0$ ) channels, the contact components of the (partial-wave expanded) potential with  $JT$  and  $S = 0$  read:

$$v_{J,J}^{JT0}(p', p; \text{CT0}/2) = \frac{1}{8\pi} \int_{-1}^1 dz P_J(z) \left[ D_1 + D_2 (p'^2 + p^2) - 2 D_3 p' p z \right] C_\Lambda(p', p, z) , \quad (5.8)$$

where  $z = \hat{\mathbf{p}}' \cdot \hat{\mathbf{p}}$ ,  $P_J(z)$  is a Legendre polynomial, and the  $D_i$  denote linear combinations of the LEC's with  $D_1 = C_S - 3 C_T$ ,  $D_2 = C_1 - 3 C_3 - C_6 + (C_2 - 3 C_4 - C_7)/4$ , and  $D_3 = C_1 - 3 C_3 - C_6 - (C_2 - 3 C_4 - C_7)/4$ . The cutoff function is even in  $z$ , and therefore for even (odd)  $J$  only  $D_1$  and  $D_2$  ( $D_3$ ) contribute. In practice,  $D_1$  and  $D_2$  have been determined by fitting the ( $np$ ) singlet scattering length and effective range, and  $^1S_0$  phase shift, while  $D_3$  is determined by fitting the  $^1P_1$  phases. In the case of spin-triplet ( $S = 1$ ) channels, the

TABLE II: Values of the LEC's corresponding to cutoff parameters  $\Lambda$  in the range 500–700 MeV, obtained from fits to  $np$  phase shifts up to lab energies of 100 MeV.

|                          | $\Lambda$ (MeV) |           |           |
|--------------------------|-----------------|-----------|-----------|
|                          | 500             | 600       | 700       |
| $C_S$ (fm <sup>2</sup> ) | −4.456420       | −4.357712 | −3.863625 |
| $C_T$ (fm <sup>2</sup> ) | 0.034780        | 0.094149  | 0.234176  |
| $C_1$ (fm <sup>4</sup> ) | −0.360939       | −0.259186 | −0.268296 |
| $C_2$ (fm <sup>4</sup> ) | −1.460509       | −0.934505 | −0.835226 |
| $C_3$ (fm <sup>4</sup> ) | −0.349780       | −0.359547 | −0.389047 |
| $C_4$ (fm <sup>4</sup> ) | −1.968636       | −1.717178 | −1.724544 |
| $C_5$ (fm <sup>4</sup> ) | −0.870067       | −0.754021 | −0.695564 |
| $C_6$ (fm <sup>4</sup> ) | 0.326169        | 0.301194  | 0.348152  |
| $C_7$ (fm <sup>4</sup> ) | −0.727797       | −1.006459 | −0.955273 |

situation is slightly more complicated. For uncoupled channels with  $J > 0$ , we write

$$v_{J,J}^{JT1}(p', p; \text{CT0}/2) = \frac{1}{8\pi} \int_{-1}^1 dz \left[ P_J(z) \left[ D_4 + (D_5 + D_6) (p'^2 + p^2) - 2 (D_7 - D_8 - D_9) p' p z \right] \right. \\ \left. - \left[ P_{J-1}(z) + P_{J+1}(z) \right] (2 D_8 + D_9) p' p \right] C_\Lambda(p', p, z) , \quad (5.9)$$

while for the  $^3P_0$  channel (having  $JTS = 011$ )

$$v_{1,1}^{011}(p', p; \text{CT0}/2) = \frac{1}{8\pi} \int_{-1}^1 dz \left[ P_1(z) \left[ D_4 + (D_5 - D_6) (p'^2 + p^2) - (2 D_7 - D_9) p' p z \right] \right. \\ \left. + P_0(z) (2 D_8 - D_9) p' p \right] C_\Lambda(p', p, z) . \quad (5.10)$$

Here, the  $D_i$ 's denote the following LEC combinations:  $D_4 = C_S + C_T$ ,  $D_5 = C_1 + C_3 + (C_2 + C_4)/4$ ,  $D_6 = C_6 + C_7/4$ ,  $D_7 = C_1 + C_3 - (C_2 + C_4)/4$ ,  $D_8 = C_6 - C_7/4$ , and  $D_9 = C_5$ . In terms of these, the contact components for coupled channels are given by

$$v_{--}^{JT1}(p', p; \text{CT0}/2) = \frac{1}{8\pi} \int_{-1}^1 dz \left[ P_{J-1}(z) \left[ D_4 + \left( D_5 + \frac{D_6}{2J+1} \right) (p'^2 + p^2) - (2 D_7 - D_9) p' p z \right] \right. \\ \left. - P_J(z) \left( \frac{2 D_8}{2J+1} + D_9 \right) p' p \right] C_\Lambda(p', p, z) , \quad (5.11)$$

$$v_{++}^{JT1}(p', p; \text{CT0}/2) = \frac{1}{8\pi} \int_{-1}^1 dz \left[ P_{J+1}(z) \left[ D_4 + \left( D_5 - \frac{D_6}{2J+1} \right) (p'^2 + p^2) - (2D_7 - D_9) p' p z \right] \right. \\ \left. + P_J(z) \left( \frac{2D_8}{2J+1} - D_9 \right) p' p \right] C_\Lambda(p', p, z), \quad (5.12)$$

$$v_{+-}^{JT1}(p', p; \text{CT0}/2) = -\frac{1}{4\pi} \frac{\sqrt{J(J+1)}}{2J+1} \int_{-1}^1 dz \left[ D_6 \left[ P_{J-1}(z) p'^2 + P_{J+1}(z) p^2 \right] \right. \\ \left. - 2D_8 P_J(z) p' p \right] C_\Lambda(p', p, z), \quad (5.13)$$

where  $L = \pm$  is a shorthand for  $L = J \pm 1$ , and the off-diagonal matrix element with  $-+$  is obtained from  $v_{+-}^{JT1}(p', p; \text{CT0}/2)$  by exchanging  $p' \rightleftharpoons p$ . The parameters  $D_4$ ,  $D_5$  and  $D_6$  are then determined by fitting the deuteron binding energy, spin-triplet scattering length and effective range, and  ${}^3\text{S}_1$ - ${}^3\text{D}_1$  phases and mixing angle—the contributions of terms proportional to  $D_7$ ,  $D_8$ , and  $D_9$  vanish in this channel. On the other hand, only the latter enter into the  ${}^3\text{P}_{J=0,1,2}$  channels, and the associated phases can then be used to fit  $D_7$ ,  $D_8$ , and  $D_9$ .

Results for the S- and P-wave phases used in the fits, as well as for the D-wave and peripheral F- and G-wave phases, and mixing angles  $\epsilon_{J=1,\dots,4}$  are displayed in Figs. 7–12 up to 200 MeV lab kinetic energies. Effective range expansions and deuteron properties are listed in Table III. For reference, in Figs. 9–12, following the original work by Kaiser *et al.* [31], the phases obtained by including only the one- and two-pion-exchange ( $\overline{v}^\pi$  and  $\overline{v}^{2\pi}$ , respectively) terms of the potential are also shown. These have been calculated in first order perturbation theory on the  $T$ -matrix, and hence are cutoff independent.

Overall, the quality of the fits at N<sup>2</sup>LO is comparable to that reported in Refs. [17, 37] and, more recently, in Ref. [38]. While the cutoff dependence is relatively weak for the S-wave phases beyond lab energies of 100 MeV, it becomes significant for higher partial wave phases and for the mixing angles. In particular, the F- and G-wave phases, while small because of the centrifugal barrier, nevertheless display a pronounced sensitivity to short-range physics, although there are indications [39] that inclusion of explicit  $\Delta$ -isobar degrees of freedom might reduce this sensitivity. Beyond 100 MeV, the agreement between the calculated and experimental phases is generally poor, and indeed in the  ${}^3\text{D}_3$  and  ${}^3\text{F}_4$  channels they have opposite sign. The scattering lengths are well reproduced by the fits (within  $\sim 1\%$  of the data, see Table III), however, the singlet and triplet effective ranges are both significantly underpredicted, by  $\sim 10\%$  and  $\sim 5\%$  respectively.

The deuteron S- and D-wave radial wave functions are shown in Fig. 13 along with those calculated with the Argonne  $v_{18}$  (AV18) potential [30]. The D wave is particularly sensitive to variations in the cutoff: it is pushed in as  $\Lambda$  is increased from 500 to 700 MeV, but remains considerably smaller than that of the AV18 up to internucleon distances of  $\sim 1.5$  fm, perhaps not surprisingly, since this realistic potential has a strong tensor component at short range. The static properties, *i.e.* D- to S-state ratio, mean-square-root matter radius, and magnetic moment—the binding energy is fitted—are close to the experimental values, and their variation with  $\Lambda$  is quite modest. The quadrupole moment is underpredicted

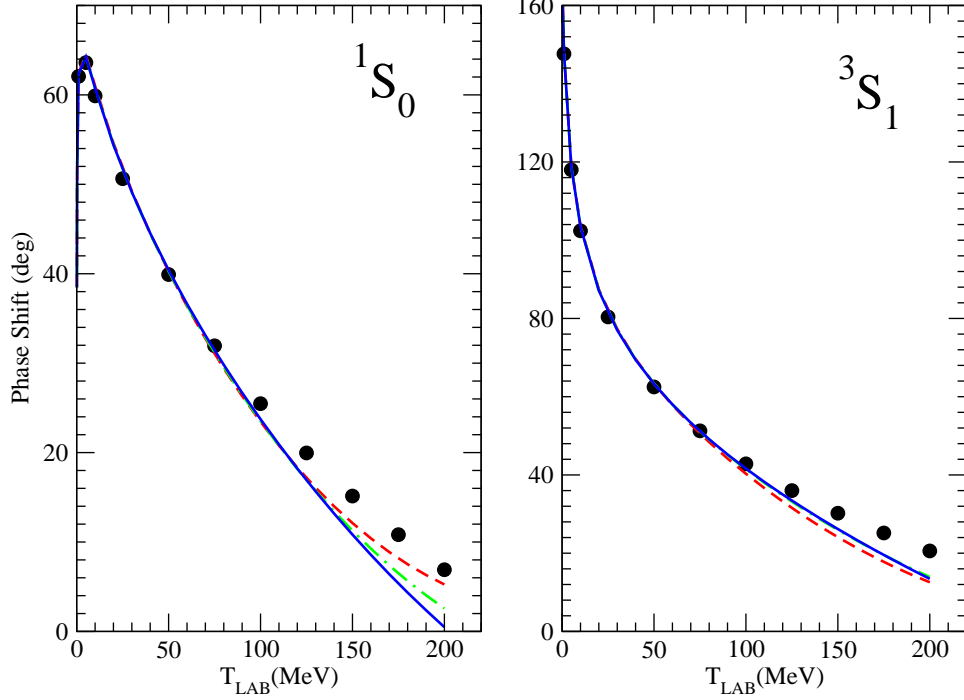


FIG. 7: (Color online) The S-wave  $np$  phase shifts, obtained with cutoff parameters  $\Lambda=500, 600$ , and  $700$  MeV, are denoted by dash (red), dot-dash (green), and solid (blue) lines, respectively. The filled circles represent the phase-shift analysis of Ref. [16].

by  $\sim 4\%$ , a pathology common, to the best of our knowledge, to all realistic potentials (including the AV18).

## VI. $N^3\text{LO}$ MAGNETIC MOMENT FROM CONTACT CURRENTS

The magnetic moment due to the contact currents originating from minimal couplings (Sec. III A) can also be separated into a Sachs term and one independent of the center-of-mass position  $\mathbf{R}$  of the two nucleons. To this end, we first note that, because of the gradients acting on the nucleon fields, the  $NN$  contact potential contains, in addition to the contribution  $v^{\text{CT}2}(\mathbf{k}, \mathbf{K})$  in Eq. (2.4), also a contribution dependent on the pair momentum  $\mathbf{P} = \mathbf{p}_1 + \mathbf{p}_2 = \mathbf{p}'_1 + \mathbf{p}'_2$ , given by

$$v_{\mathbf{P}}^{\text{CT}2}(\mathbf{k}, \mathbf{K}) = i C_1^* \frac{\boldsymbol{\sigma}_1 - \boldsymbol{\sigma}_2}{2} \cdot \mathbf{P} \times \mathbf{k} + C_2^* (\boldsymbol{\sigma}_1 \cdot \mathbf{P} \boldsymbol{\sigma}_2 \cdot \mathbf{K} - \boldsymbol{\sigma}_1 \cdot \mathbf{K} \boldsymbol{\sigma}_2 \cdot \mathbf{P}) + (C_3^* + C_4^* \boldsymbol{\sigma}_1 \cdot \boldsymbol{\sigma}_2) P^2 + C_5^* \boldsymbol{\sigma}_1 \cdot \mathbf{P} \boldsymbol{\sigma}_2 \cdot \mathbf{P}, \quad (6.1)$$

where the  $C_i^*$ 's consist of the following LEC combinations

$$\begin{aligned} C_1^* &= C'_5/2 + C'_6/2, \\ C_2^* &= 2 C'_7 - 2 C'_8 - C'_{10} + C'_{11}, \\ C_3^* &= -C'_1 + C'_2/2 - C'_3, \\ C_4^* &= -C'_9 + C'_{12}/2 + C'_{14}, \\ C_5^* &= -C'_7/2 - C'_8/2 + C'_{10}/4 + C'_{11}/4 + C'_{13}. \end{aligned} \quad (6.2)$$

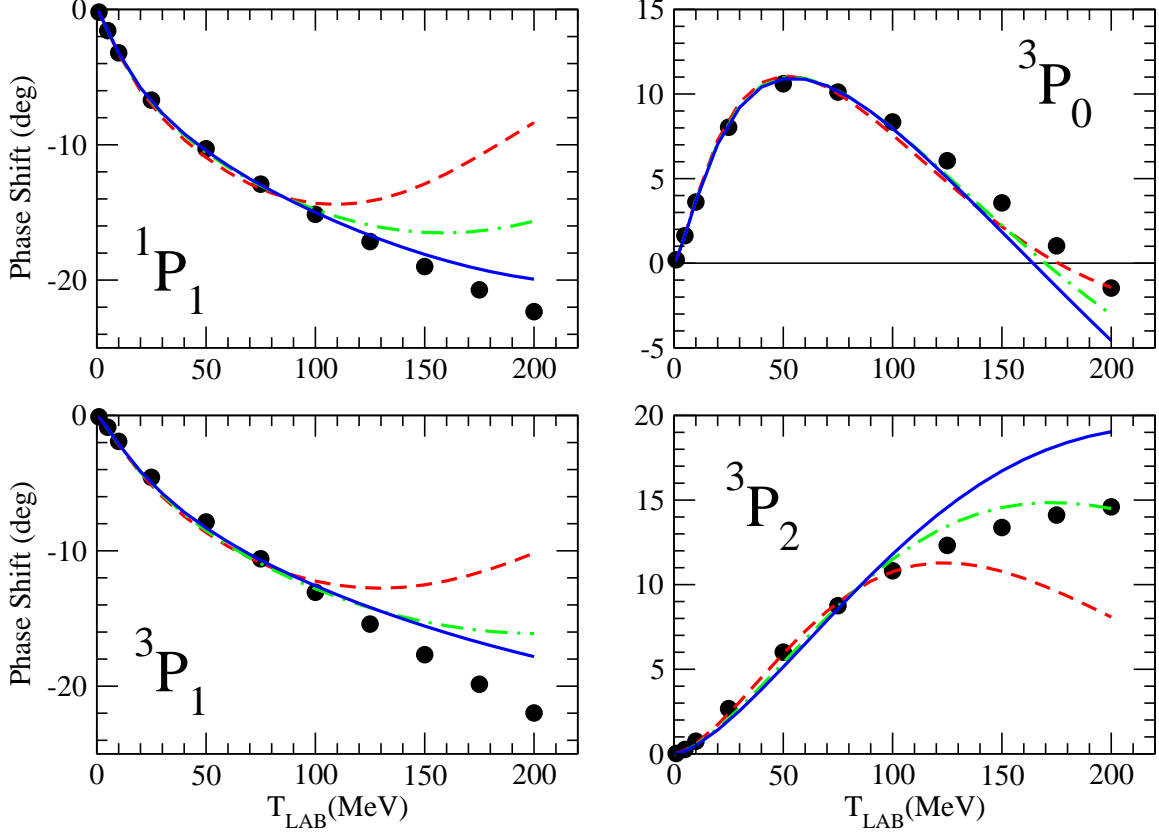


FIG. 8: (Color online) Same as in Fig. 7, but for P-wave phase shifts.

TABLE III: Singlet and triplet  $np$  scattering lengths ( $a_s$  and  $a_t$ ) and effective ranges ( $r_s$  and  $r_t$ ), and deuteron binding energy ( $B_d$ ), D- to S-state ratio ( $\eta_d$ ), root-mean-square matter radius ( $r_d$ ), magnetic moment ( $\mu_d$ ), quadrupole moment ( $Q_d$ ), and D-state probability ( $P_D$ ), obtained with  $\Lambda=500, 600$ , and  $700$  MeV, are compared to the corresponding experimental values ( $a_s$ ,  $r_s$ ,  $a_t$ , and  $r_t$  from Ref. [32],  $B_d$  from Ref. [33],  $\eta_d$  from Ref. [34],  $r_d$  and  $\mu_d$  from Ref. [35],  $Q_d$  from Ref. [36]).

|                          | $\Lambda$ (MeV) |         |         | Expt             |
|--------------------------|-----------------|---------|---------|------------------|
|                          | 500             | 600     | 700     |                  |
| $a_s$ (fm)               | -23.729         | -23.736 | -23.736 | -23.749(8)       |
| $r_s$ (fm)               | 2.528           | 2.558   | 2.567   | 2.81(5)          |
| $a_t$ (fm)               | 5.360           | 5.371   | 5.376   | 5.424(3)         |
| $r_t$ (fm)               | 1.665           | 1.680   | 1.687   | 1.760(5)         |
| $B_d$ (MeV)              | 2.2244          | 2.2246  | 2.2245  | 2.224575(9)      |
| $\eta_d$                 | 0.0267          | 0.0260  | 0.0264  | 0.0256(4)        |
| $r_d$ (fm)               | 1.943           | 1.947   | 1.951   | 1.9734(44)       |
| $\mu_d$ ( $\mu_N$ )      | 0.860           | 0.858   | 0.853   | 0.8574382329(92) |
| $Q_d$ (fm <sup>2</sup> ) | 0.275           | 0.272   | 0.279   | 0.2859(3)        |
| $P_D$ (%)                | 3.44            | 3.87    | 4.77    |                  |

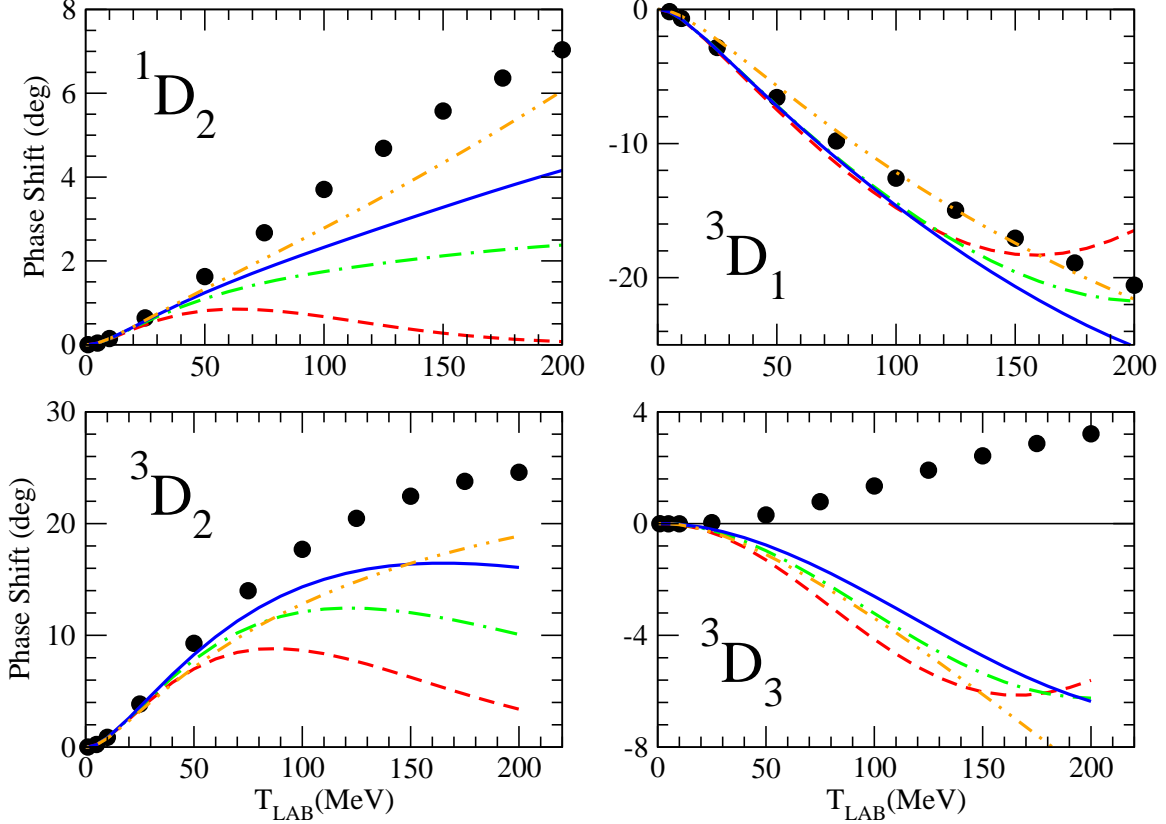


FIG. 9: (Color online) Same as in Fig. 7, but for D-wave phase shifts. The dash-double-dot (orange) line is obtained in first order perturbation theory for the  $T$ -matrix by including only the one- and two-pion-exchange parts of the  $N^2$ LO potential.

Incidentally, we observe that Eqs. (2.5) and (6.2) provide a one-to-one correspondence between the LEC's and the coefficients of the  $NN$  contact potential.

The (conserved) current  $\mathbf{j}_{\text{CT}\gamma}^{\text{N}^3\text{LO}}$  in Eq. (3.11) gives rise to a Sachs magnetic moment

$$\boldsymbol{\mu}_{\text{Sachs}}^{\text{N}^3\text{LO},\text{CT}} = -\frac{ie}{2} \left( 1 + \frac{\tau_{1,z} + \tau_{2,z}}{2} \right) \mathbf{R} \times [\mathbf{R}, v_{\mathbf{P}}^{\text{CT}2}] - \frac{ie}{4} \frac{\tau_{1,z} - \tau_{2,z}}{2} \mathbf{R} \times [\mathbf{r}, v^{\text{CT}2} + v_{\mathbf{P}}^{\text{CT}2}], \quad (6.3)$$

where the only term in  $v_{\mathbf{P}}^{\text{CT}2}$  with a non-vanishing commutator with the relative position  $\mathbf{r}$  is that proportional to  $C_2^*$ . Equation (6.3) can be easily verified by considering  $(\mathbf{R}/2) \times \mathbf{j}_{\text{CT}\gamma}^{\text{N}^3\text{LO}}(\mathbf{q} = 0)$ .

The  $M1$  operator above depends on the unknown  $C_i^*$ , which could be determined, for example, by fitting  $A=3$  bound and scattering state properties, or  $M1$  transitions in light nuclei with  $A > 2$  [40]. Instead, here we will require that they vanish, *i.e.* that the contact potential is independent of the nucleon pair momentum. To the best of our knowledge, this approximation has been adopted, albeit implicitly, in all studies of  $A > 2$  nuclei based on  $\chi$ EFT potentials. In this respect, we observe that relativistic boost corrections [41] to the rest-frame  $v^{\text{CT}2}(\mathbf{k}, \mathbf{K})$ , being proportional to  $\sim v^{\text{CT}2}(P^2/m_N^2)$ , are suppressed by two additional powers of the low momentum scale  $Q$  relative to both  $v^{\text{CT}2}(\mathbf{k}, \mathbf{K})$  and  $v_{\mathbf{P}}^{\text{CT}2}(\mathbf{k}, \mathbf{K})$ . These corrections arise from the relativistic energy-momentum relation, Lorentz contraction, and Thomas precession of the spins, and are of a different nature than the  $\mathbf{P}$ -dependent

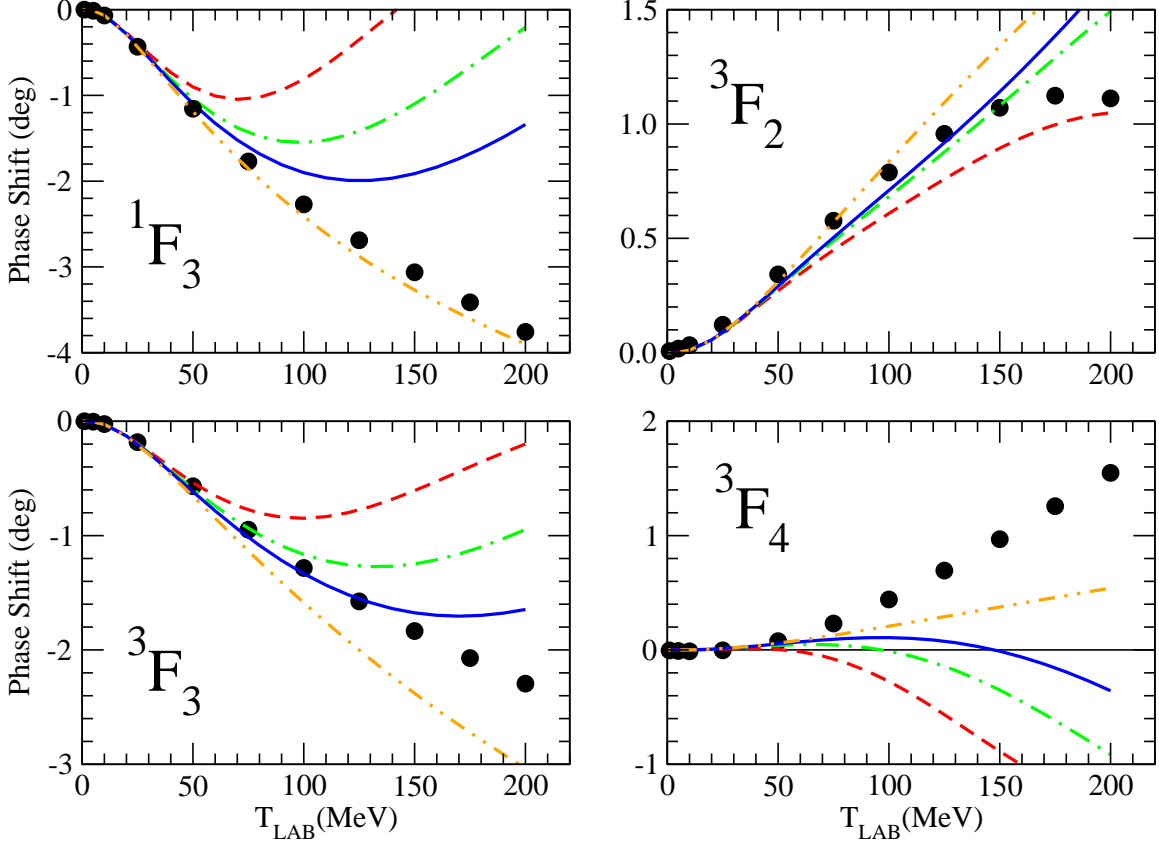


FIG. 10: (Color online) Same as in Fig. 9, but for F-wave phase shifts.

terms in  $v_{\mathbf{P}}^{\text{CT}2}(\mathbf{k}, \mathbf{K})$ , which result from the derivative couplings in the four-nucleon contact Hamiltonians.

Under the assumption above ( $C_i^* = 0$ ) and after evaluating the commutator  $[\mathbf{r}, v^{\text{CT}2}]$ , we find the Sachs magnetic moment to be given in momentum space by

$$\begin{aligned} \mu_{\text{Sachs}}^{\text{N}^3\text{LO,CT}}(\mathbf{R}, \mathbf{k}, \mathbf{K}) = & \frac{e}{4} \frac{\tau_{1,z} - \tau_{2,z}}{2} \mathbf{R} \times \left[ 2(C_2 + C_4 \boldsymbol{\sigma}_1 \cdot \boldsymbol{\sigma}_2) \mathbf{K} - i C_5 \frac{\boldsymbol{\sigma}_1 + \boldsymbol{\sigma}_2}{2} \times \mathbf{k} \right. \\ & \left. + C_7 (\boldsymbol{\sigma}_1 \boldsymbol{\sigma}_2 \cdot \mathbf{K} + \boldsymbol{\sigma}_1 \cdot \mathbf{K} \boldsymbol{\sigma}_2) \right]. \end{aligned} \quad (6.4)$$

It is determined by  $C_2$ ,  $C_4$ ,  $C_5$ , and  $C_7$ , *i.e.* by the LEC's of the momentum-dependent terms in  $v^{\text{CT}2}$  which do not commute with the charge operator. In configuration space,  $\mathbf{K}$  reduces to the relative momentum operator, and the pair correlation function  $\delta(\mathbf{r})$  is smeared over a length scale  $1/\Lambda$  ( $\Lambda$  is the high-momentum cutoff introduced in Sec. V).

The  $\mathbf{R}$ -independent contribution due to minimal couplings follows from the second term in Eq. (4.3),

$$\mu_{\text{m}}^{\text{N}^3\text{LO,CT}} = -\frac{e}{2} (C_4' + C_5') (\boldsymbol{\sigma}_1 + \boldsymbol{\sigma}_2), \quad (6.5)$$

where we have used the relation  $C_6' = -C_5'$  implied by  $C_1^* = 0$ , and have dropped a term proportional to  $(\tau_{1,z} + \tau_{2,z}) (\boldsymbol{\sigma}_1 + \boldsymbol{\sigma}_2)$ , since it vanishes when acting on antisymmetric two-nucleons states. However, the contribution due to non-minimal couplings, which only consists of translationally-invariant terms (the corresponding currents are transverse to  $\mathbf{q}$  and



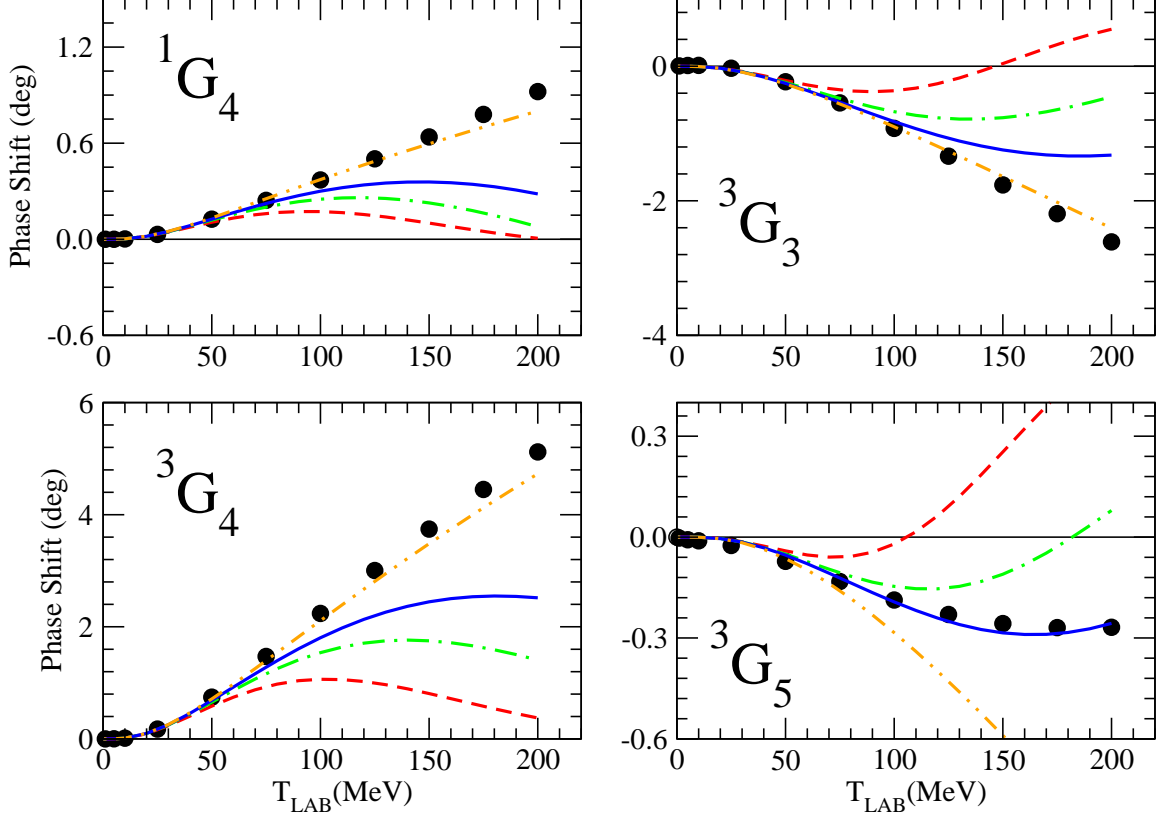


FIG. 11: (Color online) Same as in Fig. 9, but for G-wave phase shifts.

therefore unconstrained by the continuity equation), is given by

$$\mu_{\text{nm}}^{\text{N}^3\text{LO,CT}} = -e C'_{15} (\boldsymbol{\sigma}_1 + \boldsymbol{\sigma}_2) - e C'_{16} (\tau_{1,z} - \tau_{2,z}) (\boldsymbol{\sigma}_1 - \boldsymbol{\sigma}_2). \quad (6.6)$$

Hence, the  $M1$  operator due to minimal and non-minimal couplings is determined by two independent LEC's, one of which multiplies an isoscalar structure, while the other multiplies an isovector structure. The former (latter) could be determined by reproducing the deuteron magnetic moment (the cross section for  $np$  radiative capture or the isovector combination of the trinucleon magnetic moment).

### Acknowledgments

Conversations at various stages of the present work with J.L. Goity are gratefully acknowledged, as is a useful comment by J.D. Walecka in reference to the  $\text{N}^3\text{LO}$  magnetic moment operator. We wish to thank F. Gross and A. Stadler for advice relating to their phase-shift analysis, E. Epelbaum for correspondence on various aspects of the  $\text{N}^2\text{LO}$  potential, R. Machleidt for a clarification on a phase convention, and D.R. Phillips for a critical reading of the manuscript. One of the authors (R.S.) would also like to thank the Physics Department of the University of Pisa, the INFN Pisa branch, and especially the Pisa group for the support and warm hospitality extended to him on several occasions. The work of R.S. and R.B.W. is supported by the U.S. Department of Energy, Office of Nuclear Physics, under contracts DE-AC05-06OR23177 and DE-AC02-06CH11357, respectively. Some of the

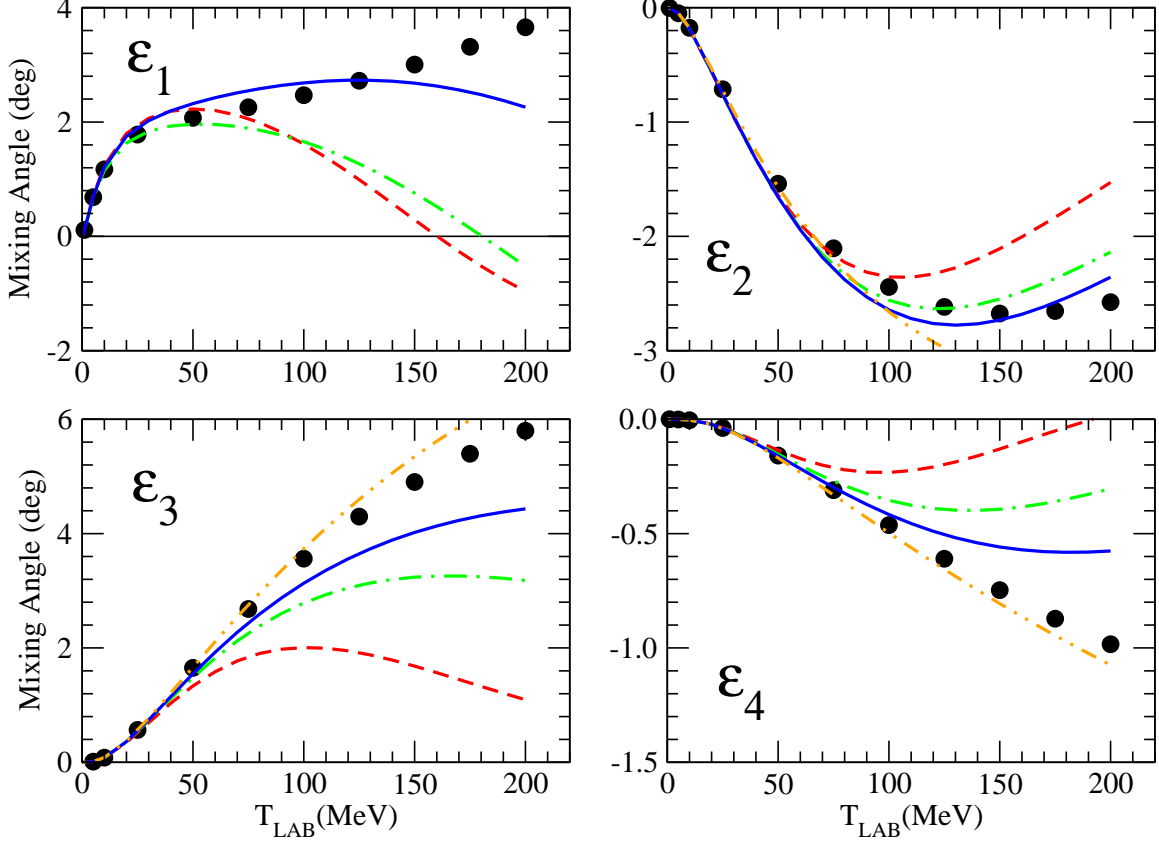


FIG. 12: (Color online) Same as in Fig. 9, but for the mixing angles  $\epsilon_J$ .

calculations were made possible by grants of computing time from the National Energy Research Supercomputer Center.

## APPENDIX A: N<sup>3</sup>LO CURRENTS FROM NON-MINIMAL COUPLINGS

External currents enter into the chiral Lagrangian either by the gauging of spacetime derivatives (minimal coupling), or through their field strengths  $F_{\mu\nu}$ , which transform covariantly under chiral symmetry. In the case of the electromagnetic current, we have both isoscalar and isovector components. In the non-relativistic limit the allowed spin-space structures, at leading order, are

$$\epsilon_{ijk} F_{ij} N^\dagger \sigma_k N N^\dagger N, \quad (\text{A1})$$

which, by time-reversal symmetry, can only be associated with the flavor structures  $\mathbf{1} \otimes \mathbf{1}$ ,  $\tau_a \otimes \tau_a$  and  $(\tau_z \otimes \mathbf{1} \pm \mathbf{1} \otimes \tau_z)$ , and

$$F_{ij} N^\dagger \sigma_i N N^\dagger \sigma_j N, \quad (\text{A2})$$

which can only be associated with the antisymmetric flavor structure  $\epsilon_{zab} \tau_a \otimes \tau_b$ . Using the Fierz-type identities for the Pauli matrices,

$$(\mathbf{1})[\mathbf{1}] = \frac{1}{2}(\mathbf{1})[\mathbf{1}] + \frac{1}{2}(\boldsymbol{\sigma}) \cdot (\boldsymbol{\sigma}), \quad (\text{A3})$$

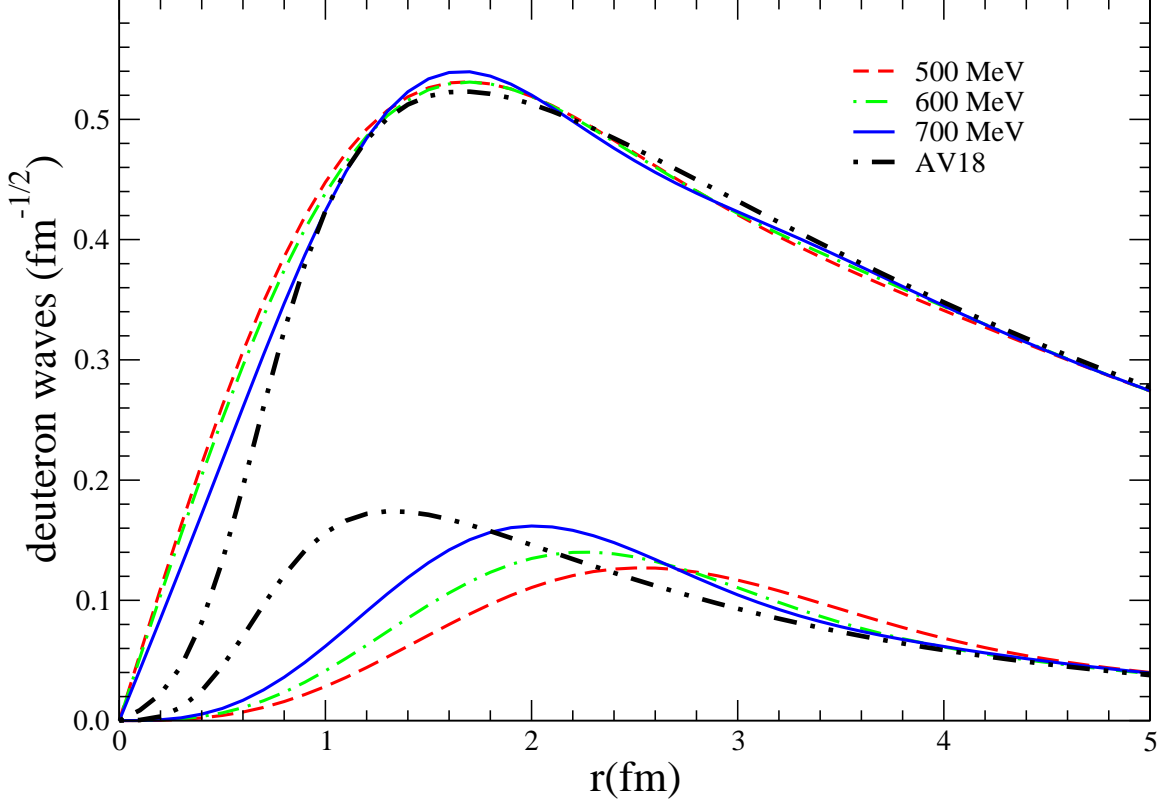


FIG. 13: (Color online) The S-wave and D-wave components of the deuteron, obtained with cutoff parameters  $\Lambda=500, 600$ , and  $700$  MeV and denoted by dash (red), dot-dash (green), and solid (blue) lines, respectively, are compared with those calculated from the Argonne  $v_{18}$  potential (dash-double-dot black lines).

$$(\mathbf{1})[\boldsymbol{\sigma}] + (\boldsymbol{\sigma})[\mathbf{1}] = (\mathbf{1})[\boldsymbol{\sigma}] + (\boldsymbol{\sigma})[\mathbf{1}] , \quad (\text{A4})$$

$$(\sigma_i) [\sigma_j] - (\sigma_j) [\sigma_i] = i \epsilon_{ijk} [(\sigma_k)[\mathbf{1}] - (\mathbf{1})[\sigma_k]] , \quad (\text{A5})$$

where  $(\cdot), [\cdot]$  denote the spinors (or isospinors)  $\chi_1^\dagger, \chi_2^\dagger, \chi_3^\dagger, \chi_4$ , we are left with two operators:

$$H_{\text{CT}\gamma, \text{nm}} = \frac{e}{2} \int d\mathbf{x} \left[ C'_{15} N^\dagger \sigma_k N N^\dagger N + C'_{16} \left( N^\dagger \sigma_k \tau_z N N^\dagger N - N^\dagger \sigma_k N N^\dagger \tau_z N \right) \right] \epsilon_{ijk} F_{ij} . \quad (\text{A6})$$

We also remark that the fourteen operators in the two-nucleon, two-derivative contact Lagrangian can be reduced to twelve, since, using partial integration, the following relation involving the vertices proportional to  $C'_4, C'_5$  and  $C'_6$  and to  $C'_7, C'_8, C'_{10}$  and  $C'_{11}$ , can be shown to hold

$$\begin{aligned} & \epsilon_{ijk} \left[ N^\dagger \nabla_i N (\nabla_j N)^\dagger \sigma_k N + (\nabla_i N)^\dagger N N^\dagger \sigma_j \nabla_k N \right] \\ &= \epsilon_{ijk} \left[ N^\dagger \sigma_k N (\nabla_i N)^\dagger \nabla_j N + N^\dagger N (\nabla_i N)^\dagger \sigma_k \nabla_j N \right] , \\ & (\delta_{ik} \delta_{jl} - \delta_{il} \delta_{jk}) \left[ N^\dagger \sigma_k \nabla_i N N^\dagger \sigma_l \nabla_j N + (\nabla_i N)^\dagger \sigma_k N (\nabla_j N)^\dagger \sigma_l N \right] \\ &= -2(\delta_{ik} \delta_{jl} - \delta_{il} \delta_{jk}) N^\dagger \sigma_k \nabla_i N (\nabla_j N)^\dagger \sigma_l N . \end{aligned} \quad (\text{A7})$$

## APPENDIX B: DIMENSIONAL REGULARIZATION OF KERNELS

In this appendix we report a list of general integration formulae [42, 43], useful to carry out the regularization of the various kernels occurring in the potential and current operators.

### 1. Useful integrals

We utilize the Feynman parameterization

$$\frac{1}{AB} = \int_0^1 dy \frac{1}{[yA + (1-y)B]^2} , \quad (\text{B1})$$

and, in order to simplify the energy factors entering the kernels, we make use of the integral representations [44]:

$$\frac{1}{\omega_+ + \omega_-} = \frac{2}{\pi} \int_0^\infty d\beta \frac{\beta^2}{(\omega_+^2 + \beta^2)(\omega_-^2 + \beta^2)} , \quad (\text{B2})$$

$$\frac{1}{\omega_+ \omega_- (\omega_+ + \omega_-)} = \frac{2}{\pi} \int_0^\infty d\beta \frac{1}{(\omega_+^2 + \beta^2)(\omega_-^2 + \beta^2)} . \quad (\text{B3})$$

Having defined

$$\int_{\mathbf{p}} \equiv \int \frac{d^d p}{(2\pi)^d} , \quad (\text{B4})$$

we have:

$$\int_{\mathbf{p}} \frac{1}{(p^2 + A)^\alpha} = \frac{1}{(4\pi)^{d/2}} \frac{\Gamma(\alpha - d/2)}{\Gamma(\alpha)} A^{-(\alpha - d/2)} , \quad (\text{B5})$$

$$\int_{\mathbf{p}} \frac{p^2}{(p^2 + A)^\alpha} = \frac{1}{(4\pi)^{d/2}} \frac{d}{2} \frac{\Gamma(\alpha - d/2 - 1)}{\Gamma(\alpha)} A^{-(\alpha - d/2 - 1)} , \quad (\text{B6})$$

$$\int_{\mathbf{p}} \frac{p^4}{(p^2 + A)^\alpha} = \frac{1}{(4\pi)^{d/2}} \frac{d(d+2)}{4} \frac{\Gamma(\alpha - d/2 - 2)}{\Gamma(\alpha)} A^{-(\alpha - d/2 - 2)} , \quad (\text{B7})$$

where  $\Gamma(z)$  is the  $\Gamma$ -function satisfying  $z\Gamma(z) = \Gamma(z+1)$ , with asymptotic behavior for  $z \rightarrow 0$  given by

$$\Gamma(z) = \frac{1}{z} - \gamma + \left( \frac{\gamma^2}{2} + \frac{\pi^2}{12} \right) z + O(z^2) , \quad (\text{B8})$$

and  $\gamma \approx 0.5772$  is the Euler-Mascheroni constant. However, we note that, in order to preserve physical dimensions, a renormalization scale  $\mu$  has to be introduced, and therefore a factor  $\mu^{3-d}$  should be understood in Eq. (B4).

Finally, we use the following relations [45] to evaluate

$$\int dx \ln |x^2 - a^2| = x \ln |x^2 - a^2| - 2x + a \ln \left| \frac{x+a}{x-a} \right| , \quad (\text{B9})$$

$$\int dx x^2 \ln |x^2 - a^2| = \frac{1}{3} \left( x^3 \ln |x^2 - a^2| - \frac{2}{3} x^3 - 2a^2 x + a^3 \ln \left| \frac{x+a}{x-a} \right| \right) , \quad (\text{B10})$$

$$\int dx x^4 \ln |x^2 - a^2| = \frac{1}{5} \left( x^5 \ln |x^2 - a^2| - \frac{2}{5} x^5 - \frac{2}{3} a^2 x^3 - 2a^4 x + a^5 \ln \left| \frac{x+a}{x-a} \right| \right) . \quad (\text{B11})$$

## 2. Regularization of the kernels

As an example, we sketch the regularization of the kernel  $I^{(0)}(k)$ , given by

$$I^{(0)}(k) = \int_{\mathbf{p}} \frac{1}{\omega_+ \omega_- (\omega_+ + \omega_-)} = \frac{2}{\pi} \int_{\mathbf{p}} \int_0^\infty d\beta \frac{1}{(\omega_+^2 + \beta^2)(\omega_-^2 + \beta^2)}, \quad (\text{B12})$$

where  $\omega_\pm = \sqrt{(\mathbf{p} \pm \mathbf{k})^2 + 4m_\pi^2}$ . Using the Feynman integral parameterization of Eq. (B1) with  $A = \omega_+^2 + \beta^2$  and  $B = \omega_-^2 + \beta^2$ , we obtain

$$\begin{aligned} I^{(0)}(k) &= \frac{2}{\pi} \int_{\mathbf{p}} \int_0^1 dy \int_0^\infty d\beta \left[ [\mathbf{p} + (2y-1)\mathbf{k}]^2 + 4[m_\pi^2 - y(y-1)k^2] + \beta^2 \right]^{-2} \\ &= \frac{1}{2} \int_{\mathbf{p}} \int_0^1 dy \left[ p^2 + 4[m_\pi^2 - y(y-1)k^2] \right]^{-3/2}, \end{aligned} \quad (\text{B13})$$

where in the second line we have also shifted the integration variable  $\mathbf{p} \rightarrow \mathbf{p} + (2y-1)\mathbf{k}$ . The integral over  $\mathbf{p}$  is reduced to the form given in Eq. (B5) with  $d = 3$ ,  $\alpha = 3/2$ , and  $A = 4[m_\pi^2 - y(y-1)k^2]$ . With this choice of  $d$  and  $\alpha$ , we are left with a  $\Gamma$ -function of vanishing argument. In order to isolate the divergent part of the integral, we set  $d = 3 - \epsilon$  and study its asymptotic behavior for  $\epsilon \rightarrow 0^+$ . Using

$$\Gamma\left(\frac{\epsilon}{2}\right) = \frac{2}{\epsilon} - \gamma + O(\epsilon), \quad (\text{B14})$$

$$\Gamma\left(\frac{3}{2}\right) = \frac{\sqrt{\pi}}{2}, \quad (\text{B15})$$

$$\left(\frac{A}{4\pi}\right)^{-\epsilon/2} = 1 - \frac{\epsilon}{2} \ln \frac{A}{4\pi} + O(\epsilon^2), \quad (\text{B16})$$

we find, neglecting  $O(\epsilon)$  terms,

$$I^{(0)}(k) = \frac{1}{8\pi^2} \left( \ln \pi + \frac{2}{\epsilon} - \gamma \right) - \frac{1}{8\pi^2} \int_0^1 dy \ln \left[ \frac{m_\pi^2}{\mu^2} - y(y-1) \frac{k^2}{\mu^2} \right]. \quad (\text{B17})$$

After setting  $y \rightarrow (x+1)/2$  and making use of Eq. (B9), we obtain:

$$I^{(0)}(k) = -\frac{1}{8\pi^2} \left( \frac{s}{k} \ln \frac{s+k}{s-k} - \frac{2}{\epsilon} + \gamma - \ln \pi + \ln \frac{m_\pi^2}{\mu^2} - 2 \right), \quad (\text{B18})$$

where  $s = \sqrt{4m_\pi^2 + k^2}$ .

The kernels

$$I^{(2)}(k) = \int_{\mathbf{p}} \frac{p^2}{\omega_+ \omega_- (\omega_+ + \omega_-)}, \quad (\text{B19})$$

$$I_{ij}^{(2)}(k) = \int_{\mathbf{p}} \frac{p_i p_j}{\omega_+ \omega_- (\omega_+ + \omega_-)}, \quad (\text{B20})$$

can be easily evaluated as shown above. We find:

$$I^{(2)}(k) = \frac{1}{24\pi^2} \left[ \frac{2s^3}{k} \ln \frac{s+k}{s-k} + 2k^2 \left( -\frac{2}{\epsilon} + \gamma - \ln \pi + \ln \frac{m_\pi^2}{\mu^2} - \frac{5}{3} \right) \right]$$

$$+ 18 m_\pi^2 \left( -\frac{2}{\epsilon} + \gamma - \ln \pi + \ln \frac{m_\pi^2}{\mu^2} - \frac{11}{9} \right) \Big], \quad (\text{B21})$$

$$\begin{aligned} I_{ij}^{(2)}(k) &= \frac{1}{24 \pi^2} \delta_{ij} \left[ \frac{s^3}{k} \ln \frac{s+k}{s-k} + k^2 \left( -\frac{2}{\epsilon} + \gamma - \ln \pi + \ln \frac{m_\pi^2}{\mu^2} - 2 \right) \right. \\ &\quad \left. + 6 m_\pi^2 \left( -\frac{2}{\epsilon} + \gamma - \ln \pi + \ln \frac{m_\pi^2}{\mu^2} - \frac{5}{3} \right) \right] \\ &\quad - \frac{1}{24 \pi^2} \frac{k_i k_j}{k^2} \left[ \frac{s^3}{k} \ln \frac{s+k}{s-k} + k^2 \left( -\frac{2}{\epsilon} + \gamma - \ln \pi + \ln \frac{m_\pi^2}{\mu^2} - \frac{8}{3} \right) - 8 m_\pi^2 \right]. \end{aligned} \quad (\text{B22})$$

Next, we note that

$$f(\omega_+, \omega_-) \equiv \frac{\omega_+^2 + \omega_+ \omega_- + \omega_-^2}{\omega_+^3 \omega_-^3 (\omega_+ + \omega_-)} = -\frac{1}{2} \frac{d}{d m_\pi^2} \frac{1}{\omega_+ \omega_- (\omega_+ + \omega_-)}, \quad (\text{B23})$$

from which we obtain:

$$J^{(0)}(k) = \int_{\mathbf{p}} f(\omega_+, \omega_-) = \frac{1}{8 \pi^2} \frac{1}{k s} \ln \frac{s+k}{s-k}, \quad (\text{B24})$$

$$J^{(2)}(k) = \int_{\mathbf{p}} p^2 f(\omega_+, \omega_-) = -\frac{1}{8 \pi^2} \left[ \frac{2 s}{k} \ln \frac{s+k}{s-k} + 3 \left( -\frac{2}{\epsilon} + \gamma - \ln \pi + \ln \frac{m_\pi^2}{\mu^2} - \frac{2}{3} \right) \right], \quad (\text{B25})$$

$$\begin{aligned} J_{ij}^{(2)}(k) &= \int_{\mathbf{p}} p_i p_j f(\omega_+, \omega_-) = -\frac{1}{8 \pi^2} \delta_{ij} \left[ \frac{s}{k} \ln \frac{s+k}{s-k} + \left( -\frac{2}{\epsilon} + \gamma - \ln \pi + \ln \frac{m_\pi^2}{\mu^2} - \frac{4}{3} \right) \right] \\ &\quad + \frac{1}{8 \pi^2} \frac{k_i k_j}{k^2} \left( \frac{s}{k} \ln \frac{s+k}{s-k} - 2 \right), \end{aligned} \quad (\text{B26})$$

$$\begin{aligned} J^{(4)}(k) &= \int_{\mathbf{p}} p^4 f(\omega_+, \omega_-) = \frac{1}{8 \pi^2} \left[ \frac{8 s^3}{3 k} \ln \frac{s+k}{s-k} + 30 m_\pi^2 \left( -\frac{2}{\epsilon} + \gamma - \ln \pi + \ln \frac{m_\pi^2}{\mu^2} - \frac{29}{45} \right) \right. \\ &\quad \left. + \frac{5}{3} k^2 \left( -\frac{2}{\epsilon} + \gamma - \ln \pi + \ln \frac{m_\pi^2}{\mu^2} - \frac{12}{5} \right) \right]. \end{aligned} \quad (\text{B27})$$

The set of kernels involving the energy factor

$$\frac{2 \omega_+ + \omega_-}{2 \omega_+^3 \omega_- (\omega_+ + \omega_-)^2}$$

can be reduced to those of type  $J^{(2n)}(k)$  by noting that

$$\int_{\mathbf{p}} \frac{2 \omega_+ + \omega_-}{2 \omega_+^3 \omega_- (\omega_+ + \omega_-)^2} = \frac{1}{4} \int_{\mathbf{p}} \frac{\omega_+^2 + \omega_+ \omega_- + \omega_-^2}{\omega_+^3 \omega_-^3 (\omega_+ + \omega_-)} = \frac{1}{4} J^{(0)}(k), \quad (\text{B28})$$

and similarly for  $J^{(2)}(k)$ ,  $J_{ij}^{(2)}(k)$ ,  $J^{(4)}(k)$ .

The kernels involving the energy factor  $g(\omega_+, \omega_-)$ ,

$$\begin{aligned} g(\omega_+, \omega_-) &= \frac{3}{2} \frac{2 \omega_+ + \omega_-}{\omega_+^5 \omega_- (\omega_+ + \omega_-)^2} + \frac{\omega_+ + 2 \omega_-}{\omega_+^3 \omega_-^3 (\omega_+ + \omega_-)^2} \\ &= -\frac{1}{2} \frac{d}{d m_\pi^2} \frac{2 \omega_+ + \omega_-}{2 \omega_+^3 \omega_- (\omega_+ + \omega_-)^2}, \end{aligned} \quad (\text{B29})$$

easily follow from

$$K^{(0)}(k) = \int_{\mathbf{p}} g(\omega_+, \omega_-) = -\frac{1}{8} \frac{d}{dm_\pi^2} J^{(0)}(k) = \frac{1}{16} \frac{d^2}{d(m_\pi^2)^2} I^{(0)}(k) , \quad (\text{B30})$$

and similarly for  $K^{(2n)}(k)$ , leading to:

$$K^{(0)}(k) = \int_{\mathbf{p}} g(\omega_+, \omega_-) = \frac{1}{64\pi^2} \left[ \frac{2}{k s^3} \ln \frac{s+k}{s-k} + \frac{1}{s^2 m_\pi^2} \right] , \quad (\text{B31})$$

$$K^{(2)}(k) = \int_{\mathbf{p}} p^2 g(\omega_+, \omega_-) = \frac{1}{64\pi^2} \left[ \frac{4}{k s} \ln \frac{s+k}{s-k} + \frac{1}{m_\pi^2} \right] , \quad (\text{B32})$$

$$\begin{aligned} K_{ij}^{(2)}(k) &= \int_{\mathbf{p}} p_i p_j g(\omega_+, \omega_-) \\ &= \frac{1}{64\pi^2} \delta_{ij} \left[ \frac{2}{k s} \ln \frac{s+k}{s-k} \right] - \frac{1}{64\pi^2} \frac{k_i k_j}{k^2} \left[ \frac{2}{k s} \ln \frac{s+k}{s-k} - \frac{1}{m_\pi^2} \right] , \end{aligned} \quad (\text{B33})$$

$$\begin{aligned} K^{(4)}(k) &= \int_{\mathbf{p}} p^4 g(\omega_+, \omega_-) \\ &= -\frac{1}{64\pi^2} \left[ \frac{16 s}{k} \ln \frac{s+k}{s-k} - \frac{k^2}{m_\pi^2} + 30 \left( -\frac{2}{\epsilon} + \gamma - \ln \pi + \ln \frac{m_\pi^2}{\mu^2} \right) \right] , \end{aligned} \quad (\text{B34})$$

$$\begin{aligned} K_{ij}^{(4)}(k) &= \int_{\mathbf{p}} p^2 p_i p_j g(\omega_+, \omega_-) \\ &= -\frac{1}{64\pi^2} \delta_{ij} \left[ \frac{8 s}{k} \ln \frac{s+k}{s-k} + 10 \left( -\frac{2}{\epsilon} + \gamma - \ln \pi + \ln \frac{m_\pi^2}{\mu^2} - \frac{8}{15} \right) \right] \\ &\quad + \frac{1}{64\pi^2} \frac{k_i k_j}{k^2} \left[ \frac{8 s}{k} \ln \frac{s+k}{s-k} + \frac{k^2}{m_\pi^2} - 16 \right] . \end{aligned} \quad (\text{B35})$$

Finally, for the kernel entering diagram e) in Fig. 1, we obtain

$$\begin{aligned} L(k) &= \int_{\mathbf{p}} \frac{(\omega_+ - \omega_-)^2}{\omega_+ \omega_- (\omega_+ + \omega_-)} = \int_{\mathbf{p}} \left[ -\frac{4}{(\omega_+ + \omega_-)} + \frac{2}{\omega_+} \right] \\ &= -\frac{1}{6\pi^2} \left[ \frac{s^3}{k} \ln \frac{s+k}{s-k} - 8 m_\pi^2 + k^2 \left( -\frac{2}{\epsilon} + \gamma - \ln \pi + \ln \frac{m_\pi^2}{\mu^2} - \frac{8}{3} \right) \right] , \end{aligned} \quad (\text{B36})$$

while for the constants  $M^{(n)}$  entering Eqs. (2.19)–(2.20),

$$M^{(1)} = \int_{\mathbf{p}} \frac{1}{\omega_p} = \frac{m_\pi^2}{8\pi^2} \left( -\frac{2}{\epsilon} + \gamma - \ln 4\pi + \ln \frac{m_\pi^2}{\mu^2} - 1 \right) , \quad (\text{B37})$$

$$M^{(3)} = \int_{\mathbf{p}} \frac{p^2}{\omega_p^3} = \frac{3 m_\pi^2}{8\pi^2} \left( -\frac{2}{\epsilon} + \gamma - \ln 4\pi + \ln \frac{m_\pi^2}{\mu^2} - \frac{1}{3} \right) . \quad (\text{B38})$$

## APPENDIX C: ONE-LOOP TWO-BODY CURRENTS

In this appendix we list the expressions for the one-loop currents derived in Ref. [7]. Referring to Fig. 3, we have:

$$\text{type a)} = -2i \frac{e g_A^2}{F_\pi^4} \int \frac{2 \tau_{2,z} (\boldsymbol{\sigma}_1 \times \mathbf{q}_2) + (\boldsymbol{\tau}_1 \times \boldsymbol{\tau}_2)_z \mathbf{q}_2}{\omega_1 \omega_2 (\omega_1 + \omega_2)} + 1 \rightleftharpoons 2 , \quad (\text{C1})$$

$$\begin{aligned} \text{type b)} &= 2i \frac{e g_A^2}{F_\pi^4} \int \frac{\mathbf{q}_1 - \mathbf{q}_3}{\omega_1 \omega_2 \omega_3} \frac{\omega_1 + \omega_2 + \omega_3}{(\omega_1 + \omega_2)(\omega_1 + \omega_3)(\omega_2 + \omega_3)} \left[ (\boldsymbol{\tau}_1 \times \boldsymbol{\tau}_2)_z \mathbf{q}_1 \cdot \mathbf{q}_2 \right. \\ &\quad \left. - 2 \tau_{2,z} \boldsymbol{\sigma}_1 \cdot (\mathbf{q}_1 \times \mathbf{q}_2) \right] + 1 \rightleftharpoons 2, \end{aligned} \quad (\text{C2})$$

$$\text{type c)} = -i \frac{e}{2 F_\pi^4} (\boldsymbol{\tau}_1 \times \boldsymbol{\tau}_2)_z \int \frac{\mathbf{q}_1 - \mathbf{q}_3}{\omega_1 \omega_3} \frac{\omega_2(\omega_1 + \omega_2 + \omega_3) - 3 \omega_1 \omega_3}{(\omega_1 + \omega_2)(\omega_1 + \omega_3)(\omega_2 + \omega_3)}, \quad (\text{C3})$$

$$\begin{aligned} \text{type d)} &= -2i \frac{e g_A^4}{F_\pi^4} \int \frac{\omega_1^2 + \omega_2^2 + \omega_1 \omega_2}{\omega_1^3 \omega_2^3 (\omega_1 + \omega_2)} \left[ (\boldsymbol{\tau}_1 \times \boldsymbol{\tau}_2)_z \mathbf{q}_2 (\mathbf{q}_1 \cdot \mathbf{q}_2) + 2 \tau_{2,z} \mathbf{q}_1 \cdot \mathbf{q}_2 (\boldsymbol{\sigma}_1 \times \mathbf{q}_2) \right. \\ &\quad \left. + 2 \tau_{1,z} \mathbf{q}_2 \boldsymbol{\sigma}_2 \cdot (\mathbf{q}_1 \times \mathbf{q}_2) \right] + 1 \rightleftharpoons 2, \end{aligned} \quad (\text{C4})$$

$$\begin{aligned} \text{type e)} &= 2i \frac{e g_A^4}{F_\pi^4} \int (\mathbf{q}_1 - \mathbf{q}_3) f(\omega_1, \omega_2, \omega_3) \left[ (\boldsymbol{\tau}_1 \times \boldsymbol{\tau}_2)_z (\mathbf{q}_1 \cdot \mathbf{q}_2)(\mathbf{q}_2 \cdot \mathbf{q}_3) \right. \\ &\quad \left. + 2 \tau_{2,z} (\mathbf{q}_2 \cdot \mathbf{q}_3) \boldsymbol{\sigma}_1 \cdot (\mathbf{q}_2 \times \mathbf{q}_1) + 2 \tau_{1,z} (\mathbf{q}_1 \cdot \mathbf{q}_2) \boldsymbol{\sigma}_2 \cdot (\mathbf{q}_3 \times \mathbf{q}_2) \right], \end{aligned} \quad (\text{C5})$$

$$\text{type g)} = 2i \frac{e g_A^2 C_T}{F_\pi^2} (\boldsymbol{\tau}_1 \times \boldsymbol{\tau}_2)_z \int \frac{\mathbf{q}_1 - \mathbf{q}_2}{\omega_1^3 \omega_2^3} \frac{\omega_1^2 + \omega_1 \omega_2 + \omega_2^2}{\omega_1 + \omega_2} (\boldsymbol{\sigma}_1 \cdot \mathbf{q}_2)(\boldsymbol{\sigma}_2 \cdot \mathbf{q}_1), \quad (\text{C6})$$

$$\begin{aligned} \text{type i)} &= i \frac{e g_A^2}{F_\pi^2} \tau_{1,z} \int \frac{\mathbf{q}_1 - \mathbf{q}_2}{\omega_1^3 \omega_2^3} \frac{\omega_1^2 + \omega_1 \omega_2 + \omega_2^2}{\omega_1 + \omega_2} \left[ C_S \boldsymbol{\sigma}_1 \cdot (\mathbf{q}_1 \times \mathbf{q}_2) \right. \\ &\quad \left. - C_T \boldsymbol{\sigma}_2 \cdot (\mathbf{q}_1 \times \mathbf{q}_2) \right] + 1 \rightleftharpoons 2, \end{aligned} \quad (\text{C7})$$

where the  $\mathbf{q}_i$ 's and  $\omega_i = (q_i^2 + m_\pi^2)^{1/2}$  denote the momenta (with the flow as indicated in the figure) and energies of the exchanged pions, and the integration is on any one of the  $\mathbf{q}_i$ 's, the remaining  $\mathbf{q}_j$ 's with  $j \neq i$  being fixed by momentum-conserving  $\delta$ -functions. Lastly, the function  $f(\omega_1, \omega_2, \omega_3)$  in the type e) current is defined as

$$\begin{aligned} f(\omega_1, \omega_2, \omega_3) &= \frac{1}{\omega_1 \omega_2 \omega_3 (\omega_1 + \omega_2)(\omega_1 + \omega_3)(\omega_2 + \omega_3)} \left[ \frac{\omega_1 \omega_2 + \omega_2 \omega_3 + \omega_1 \omega_3}{\omega_1 \omega_2 \omega_3} \right. \\ &\quad \left. + \frac{(\omega_1 + \omega_2)(\omega_2 + \omega_3)(\omega_1^2 + \omega_3^2)}{\omega_1^2 \omega_2 \omega_3^2} + \frac{\omega_2}{\omega_1 \omega_3} + \frac{\omega_1 + \omega_2 + \omega_3}{\omega_2^2} \right]. \end{aligned} \quad (\text{C8})$$

## APPENDIX D: MAGNETIC MOMENTS FROM LOOP CURRENTS

In this appendix we list the translationally invariant contributions to the magnetic moment—second term in Eq. (4.3)—associated with currents a)-e) and i) in Fig. 3. The contributions of currents c) and g) vanish, while those of currents a), d), and i) read:

$$\begin{aligned} \bar{\mu}_a^{\text{N}^3\text{LO}}(\mathbf{k}) &= \frac{e g_A^2}{8 \pi^2 F_\pi^4} \tau_{2,z} G(k) \left[ \left( 1 - \frac{2 m_\pi^2}{4 m_\pi^2 + k^2} \right) \boldsymbol{\sigma}_1 + \frac{2 m_\pi^2}{4 m_\pi^2 + k^2} \frac{\mathbf{k} \boldsymbol{\sigma}_1 \cdot \mathbf{k}}{k^2} \right] \\ &\quad + \frac{e g_A^2}{8 \pi^2 F_\pi^4} \tau_{2,z} \left( \boldsymbol{\sigma}_1 - \frac{\mathbf{k} \boldsymbol{\sigma}_1 \cdot \mathbf{k}}{k^2} \right) + 1 \rightleftharpoons 2, \end{aligned} \quad (\text{D1})$$

$$\begin{aligned} \bar{\mu}_d^{\text{N}^3\text{LO}}(\mathbf{k}) &= -\frac{e g_A^4}{8 \pi^2 F_\pi^4} \tau_{2,z} G(k) \left[ \left[ 1 - \frac{2 m_\pi^2}{4 m_\pi^2 + k^2} - \frac{8 m_\pi^4}{(4 m_\pi^2 + k^2)^2} \right] \boldsymbol{\sigma}_1 \right. \\ &\quad \left. + \left[ -\frac{2 m_\pi^2}{4 m_\pi^2 + k^2} + \frac{8 m_\pi^4}{(4 m_\pi^2 + k^2)^2} \right] \frac{\mathbf{k} \boldsymbol{\sigma}_1 \cdot \mathbf{k}}{k^2} \right] - \frac{e g_A^4}{8 \pi^2 F_\pi^4} \tau_{2,z} \left[ \left( 1 - \frac{4 m_\pi^2}{4 m_\pi^2 + k^2} \right) \boldsymbol{\sigma}_1 \right. \end{aligned}$$



$$- \left( 1 - \frac{4 m_\pi^2}{4 m_\pi^2 + k^2} \right) \frac{\mathbf{k} \boldsymbol{\sigma}_1 \cdot \mathbf{k}}{k^2} \Big] + 1 \rightleftharpoons 2 , \quad (\text{D2})$$

$$\overline{\mu}_i^{\text{N}^3\text{LO}}(\mathbf{k}) = \frac{e g_A^2}{2 \pi^2 F_\pi^2} \tau_{1,z} (C_S \boldsymbol{\sigma}_1 - C_T \boldsymbol{\sigma}_2) + 1 \rightleftharpoons 2 . \quad (\text{D3})$$

Finally, in terms of the kernels  $J^{(n)}$  and  $K^{(n)}$ , the contributions resulting from currents b) and e) are given by

$$\mu_b^{\text{N}^3\text{LO}}(\mathbf{k}) = \frac{e g_A^2}{2 F_\pi^4} \tau_{2,z} \left[ \left[ J_{ij}^{(2)}(k) - k_i k_j J^{(0)}(k) \right] \sigma_{1,j} - \left[ J^{(2)}(k) - k^2 J^{(0)}(k) \right] \boldsymbol{\sigma}_1 \right] + 1 \rightleftharpoons 2 , \quad (\text{D4})$$

$$\begin{aligned} \mu_e^{\text{N}^3\text{LO}}(\mathbf{k}) &= \frac{2 e g_A^4}{F_\pi^4} \tau_{2,z} \left[ \left[ K^{(4)}(k) - 2 k^2 K^{(2)}(k) + k^4 K^{(0)}(k) \right] \boldsymbol{\sigma}_1 - 4 \epsilon_{ijk} k_k (\boldsymbol{\sigma}_1 \times \mathbf{k})_l K_{jl}^{(2)}(k) \right. \\ &\quad \left. - \left[ K_{ij}^{(4)}(k) - k^2 K_{ij}^{(2)}(k) - k_i k_j K^{(2)}(k) + k_i k_j k^2 K^{(0)}(k) \right] \sigma_{1,j} \right] + 1 \rightleftharpoons 2 , \end{aligned} \quad (\text{D5})$$

from which the renormalized operators follow as

$$\begin{aligned} \overline{\mu}_b^{\text{N}^3\text{LO}}(\mathbf{k}) &= \frac{e g_A^2}{8 \pi^2 F_\pi^4} \tau_{2,z} G(k) \left[ \left( 1 - \frac{2 m_\pi^2}{4 m_\pi^2 + k^2} \right) \boldsymbol{\sigma}_1 + \frac{2 m_\pi^2}{4 m_\pi^2 + k^2} \frac{\mathbf{k} \boldsymbol{\sigma}_1 \cdot \mathbf{k}}{k^2} \right] \\ &\quad - \frac{e g_A^2}{8 \pi^2 F_\pi^4} \tau_{2,z} \frac{\mathbf{k} \boldsymbol{\sigma}_1 \cdot \mathbf{k}}{k^2} + 1 \rightleftharpoons 2 , \end{aligned} \quad (\text{D6})$$

$$\begin{aligned} \overline{\mu}_e^{\text{N}^3\text{LO}}(\mathbf{k}) &= - \frac{e g_A^4}{8 \pi^2 F_\pi^4} \tau_{2,z} G(k) \left[ \left[ 1 + \frac{6 m_\pi^2}{4 m_\pi^2 + k^2} - \frac{8 m_\pi^4}{(4 m_\pi^2 + k^2)^2} \right] \boldsymbol{\sigma}_1 \right. \\ &\quad + \left[ 4 - \frac{10 m_\pi^2}{4 m_\pi^2 + k^2} + \frac{8 m_\pi^4}{(4 m_\pi^2 + k^2)^2} \right] \frac{\mathbf{k} \boldsymbol{\sigma}_1 \cdot \mathbf{k}}{k^2} \Big] - \frac{e g_A^4}{8 \pi^2 F_\pi^4} \tau_{2,z} \left[ \left( 1 - \frac{4 m_\pi^2}{4 m_\pi^2 + k^2} \right) \boldsymbol{\sigma}_1 \right. \\ &\quad \left. - \left( 5 - \frac{4 m_\pi^2}{4 m_\pi^2 + k^2} \right) \frac{\mathbf{k} \boldsymbol{\sigma}_1 \cdot \mathbf{k}}{k^2} \right] + 1 \rightleftharpoons 2 . \end{aligned} \quad (\text{D7})$$

## APPENDIX E: RECOIL CORRECTIONS

Consider the set of time-ordered diagrams, displayed in Fig. 14 and denoted as type i) in Fig. 4. It is easily seen that recoil corrections in diagrams a)+b) and i)+j) cancel out the contributions associated with diagrams c)+d) and k)+l), respectively, so that the expression for type i) diagrams in Fig. 4—which happens to vanish—results from diagrams e)-h). Let  $N$  denote the product of the four vertices in diagrams a)-d); then the contribution of diagrams a)+b) is given by

$$\begin{aligned} \text{a) + b) of Fig. 14} &= \frac{N}{(E_i - E'_p - E_2 + i\eta)(E_i - E_p - E_2 - \omega_1 + i\eta)} \times \\ &\quad \left[ \frac{1}{E_i - E'_1 - E_2 - \omega_2 + i\eta} + \frac{1}{E_i - E'_p - E'_2 - \omega_2 + i\eta} \right] , \end{aligned} \quad (\text{E1})$$

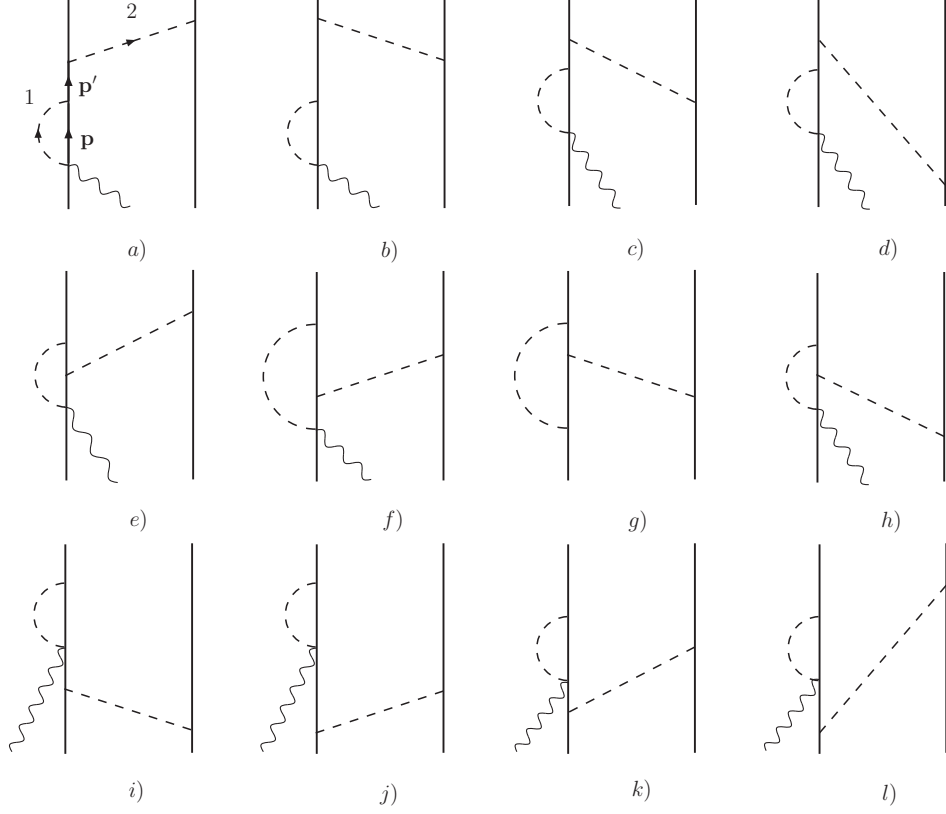


FIG. 14: Set of time-ordered diagrams for the contribution illustrated by the single diagram i) in Fig. 4. Notation as in Fig. 2.

where the labeling of the momenta is as in panel a), and  $E_p$  and  $E'_p$  are the energies of the intermediate nucleons. The expression in square brackets above can be expanded as

$$\left[ \dots \right] \simeq -\frac{1}{\omega_2} \left[ 2 + \frac{E_i - E'_p - E_2}{\omega_2} \right], \quad (\text{E2})$$

where use has been made of (overall) energy conservation,  $E_i = E'_1 + E'_2$ , and hence

$$\text{a) + b) of Fig. 14} = (\text{terms in iterated LS equation}) - \frac{N}{\omega_2^2 (E_i - E_p - E_2 - \omega_1 + i\eta)}. \quad (\text{E3})$$

The second term above in the static limit reduces to  $N/(\omega_1 \omega_2^2)$ , which exactly cancels the contribution of diagrams c)+d). These exact cancellations persist also in the k)-l) as well as u)-v) type diagrams of Figs. 4 and 5, so that in computing their contributions we only take into account the subset of (twenty, see below) time-ordered diagrams of topology as shown in those figures.

For the type j) contribution we find that the cancellation between irreducible and recoil-corrected reducible diagrams is only partial, and the result given in Eq. (3.36) corresponds to taking into account only the irreducible diagrams illustrated in Fig. 15 (the same subset considered in the evaluation of type u)-v) above). However, the remaining irreducible and recoil-corrected reducible diagrams produce an additional contribution of the form

$$e \frac{g_A^4}{F_\pi^4} N_{ij}(q) \left[ (\boldsymbol{\tau}_1 \times \boldsymbol{\tau}_2)_z (\mathbf{q} \times \mathbf{k}_2)_j + \tau_{2,z} [\mathbf{q} \times (\boldsymbol{\sigma}_1 \times \mathbf{k}_2)]_j \right] \frac{\boldsymbol{\sigma}_2 \cdot \mathbf{k}_2}{\omega_{k_2}^2}$$

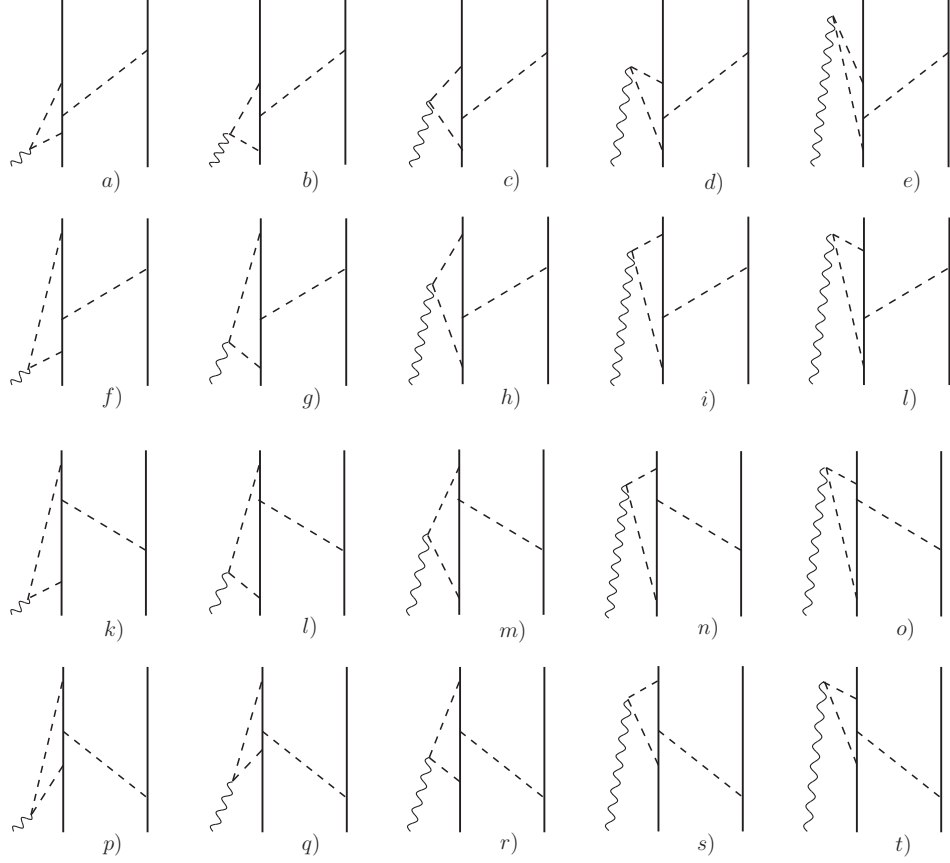


FIG. 15: Subset of time-ordered diagrams for the contribution illustrated by the single diagram j) in Fig. 4. See text for discussion. Notation as in Fig. 2.

$$+ e \frac{g_A^4}{2F_\pi^4} N_i(q) \tau_{2,z} \frac{\boldsymbol{\sigma}_1 \cdot \mathbf{k}_2 \boldsymbol{\sigma}_2 \cdot \mathbf{k}_2}{\omega_{k_2}^2} + 1 \rightleftharpoons 2 , \quad (\text{E4})$$

where the kernels  $N_{ij}$  and  $N_i$  are

$$N_{ij}(q) = \int_{\mathbf{p}} \frac{p_i p_j}{\omega_+^2 \omega_-^2 (\omega_+ + \omega_-)} , \quad (\text{E5})$$

$$N_i(q) = \int_{\mathbf{p}} p_i (p^2 - q^2) \frac{\omega_+ - \omega_-}{\omega_+^2 \omega_-^2 (\omega_+ + \omega_-)^2} , \quad (\text{E6})$$

which, however, does not lead to a Hermitian current density, since this would require  $\mathbf{j}(\mathbf{k}_1, \mathbf{k}_2) = \mathbf{j}^\dagger(-\mathbf{k}_1, -\mathbf{k}_2)$ . We have ignored this contribution.

- 
- [1] S. Weinberg, *The Quantum Theory of Fields*, vol. II (Cambridge University Press, 1995).
  - [2] V. Bernard, N. Kaiser, and U.-G. Meissner, *Int. J. Mod. Phys. E4*, 193 (1995).
  - [3] U. van Kolck, *Prog. Part. Nucl. Phys.* **43**, 337 (1999); P. Bedaque and U. van Kolck, *Ann. Rev. Nucl. Part. Sci.* **52**, 339 (2002); E. Epelbaum, *Prog. Part. Nucl. Phys.* **57**, 654 (2006); E. Epelbaum, H.-W. Hammer, and U.-G. Meissner, *Rev. Mod. Phys.* in press, arXiv:0811.1338 (2008).

- [4] T.-S. Park, D.-P. Min, and M. Rho, Phys. Rep. **233**, 341 (1993).
- [5] T.-S. Park, D.-P. Min, and M. Rho, Nucl. Phys. **A596**, 515 (1996).
- [6] J. Carlson and R. Schiavilla, Rev. Mod. Phys. **70**, 743 (1998).
- [7] S. Pastore, R. Schiavilla, and J.L. Goity, Phys. Rev. C **78**, 064002 (2008).
- [8] S. Weinberg, Phys. Lett. **B251**, 288 (1990); Nucl. Phys. **B363**, 3 (1991); Phys. Lett. **B295**, 114 (1992).
- [9] U. van Kolck, Phys. Rev. C **49**, 2932 (1994); C. Ordóñez, L. Ray, and U. van Kolck, Phys. Rev. C **53**, 2086 (1996).
- [10] E. Epelbaum, W. Glöckle, and U.-G. Meissner, Nucl. Phys. **A637**, 107 (1998); Nucl. Phys. **A747**, 362 (2005).
- [11] Y.-H. Song, R. Lazauskas, T.-S. Park, and D.-P. Min, Phys. Lett. **B656**, 174 (2007).
- [12] Y.-H. Song, R. Lazauskas, and T.-S. Park, arXiv:0812.3834.
- [13] T.-S. Park, K. Kubodera, D.-P. Min, and M. Rho, Phys. Lett. **B472**, 232 (2000).
- [14] M. Walzl and U.-G. Meissner, Phys. Lett. **B513**, 37 (2001).
- [15] D.R. Phillips, Phys. Lett. **B567**, 12 (2003).
- [16] F. Gross and A. Stadler, Phys. Rev. C **78**, 014005 (2008).
- [17] E. Epelbaum, W. Glöckle, and U.-G. Meissner, Nucl. Phys. **A671**, 295 (2000); Eur. Phys. J. **A19**, 125 (2004); Eur. Phys. J. **A19**, 401 (2004).
- [18] V.G.J. Stoks, R.A.M. Klomp, M.C.M. Rentmeester, and J.J. deSwart, Phys. Rev. C **48**, 792 (1993).
- [19] R.H. Dalitz, Phys. Rev. **95**, 799 (1954).
- [20] R.G. Sachs, Phys. Rev. **74**, 433 (1948).
- [21] In preparation.
- [22] L.E. Marcucci, M. Viviani, R. Schiavilla, A. Kievsky, and S. Rosati, Phys. Rev. C **72**, 014001 (2005).
- [23] R. Schiavilla, R.B. Wiringa, V.R. Pandharipande, and J. Carlson, Phys. Rev. C **45**, 2628 (1992).
- [24] We had erroneously counted this term as  $N^4\text{LO}$  in an earlier version of the manuscript; we are grateful to D.R. Phillips for pointing this out.
- [25] N. Fettes, U.-G. Meissner, and S. Steininger, Nucl. Phys. **A640**, 199 (1998).
- [26] R. Schiavilla, J. Carlson, and M. Paris, Phys. Rev. C **70**, 044007 (2004).
- [27] W. Glöckle, *The Quantum Mechanical Few-Body Problem* (Springer-Verlag, Berlin, 1983).
- [28] V.G.J. Stoks, R.G.E. Timmermans, J.J. de Swart, Phys. Rev. C **47**, 512 (1993).
- [29] R.A. Arndt, R.L. Workman, and M.M. Pavan, Phys. Rev. C **49**, 2729 (1994).
- [30] R.B. Wiringa, V.G.J. Stoks, and R. Schiavilla, Phys. Rev. C **51**, 38 (1995).
- [31] N. Kaiser, R. Brockmann, and W. Weise, Nucl. Phys. **A625**, 758 (1997).
- [32] L. Koester and W. Nistler, Z. Phys. A **272**, 189 (1975).
- [33] C. van der Leun and C. Alderliesten, Nucl. Phys. **A380**, 261 (1982).
- [34] N.L. Rodning and L.D. Knutson, Phys. Rev. C **41**, 898 (1990).
- [35] P.J. Mohr and B.N. Taylor, Rev. Mod. Phys. **77**, 1 (2005).
- [36] D.M. Bishop and L.M. Cheung, Phys. Rev. A **20**, 381 (1979).
- [37] D.R. Entem and R. Machleidt, Phys. Rev. C **66**, 014002 (2002); Phys. Rev. C **68**, 041001 (2003).
- [38] C.-J. Yang, Ch. Elster, and D.R. Phillips, arXiv:0901.2663; arXiv:0905.4943.
- [39] N. Kaiser, S. Gerstendoerfer, W. Weise, Nucl. Phys. **A637**, 395 (1998).
- [40] L.E. Marcucci, M. Pervin, S.C. Pieper, R. Schiavilla, and R.B. Wiringa, Phys. Rev. C **78**,

- 065501 (2008).
- [41] J. Carlson, V.R. Pandharipande, and R. Schiavilla, Phys. Rev. C **47**, 484 (1993); J.L. Forest, V.R. Pandharipande, J. Carlson, and R. Schiavilla, Phys. Rev. C **52**, 576 (1995).
  - [42] M. Veltman, *Diagrammatica* (Cambridge University Press, Cambridge, 1994).
  - [43] M.E. Peskin and D.V. Schroeder, *An introduction to Quantum Field Theory* (Westview Press, 1995).
  - [44] Th.A. Rijken and V.G.J. Stoks, Phys. Rev. **46**, 73 (1992).
  - [45] I.S. Gradshteyn and I.M. Ryzhik, *Table of Integrals, Series, and Products* (Academic Press, 1994).